



High-order strongly nonlinear long wave approximation and solitary wave solution. Part 2. Internal waves

Wooyoung Choi†

Department of Mathematical Sciences, New Jersey Institute of Technology, Newark, NJ 07102-1982, USA

(Received 20 July 2022; revised 6 November 2022; accepted 8 November 2022)

A strongly nonlinear long-wave approximation is adopted to obtain a high-order model for large-amplitude long internal waves in a two-layer system by assuming the water depth is much smaller than the typical wavelength. When truncated at the first order, the model can be reduced to the regularized strongly nonlinear model of Choi *et al.* (*J. Fluid Mech.*, vol. 629, 2009, pp. 73–85), which lessens the Kelvin–Helmholtz instability excited by the tangential velocity jump across the interface in the inviscid Miyata–Choi–Camassa (MCC) equations. Using the second-order model, the next-order correction to the internal solitary wave solution of the MCC equations is found and its validity is examined with the Euler solution in terms of the wave profile, the effective wavelength and the velocity profile. It is shown that the correction greatly improves the comparison with the Euler solution for the whole range of wave amplitudes and no further correction is necessary for practical applications. Based on a local stability analysis, the region of stability for the second-order long-wave model is identified in the physical parameter space so that the efficient numerical scheme developed for the first-order model can be used for the second-order model.

Key words: internal waves, solitary waves, shallow water flows

1. Introduction

Nonlinear internal solitary waves propagating in density-stratified oceans are frequently observed on satellite images. As the density difference in the ocean is typically small, or $O(10^{-3})$, the gravitational effect is greatly reduced so that the amplitudes of internal solitary waves are usually large compared with the characteristic vertical length scale, such as the well-mixed surface layer thickness, as observed in numerous field and laboratory experiments (Helfrich & Melville 2006). When its density changes sharply from one value to another, the stratified ocean is often approximated by a two-layer system, for which one

† Email address for correspondence: wychoi@njit.edu

can find four characteristic lengths: a, λ , h_1 and h_2 , representing the wave amplitude, the wavelength and the top and bottom layer thicknesses, respectively. For internal solitary waves, while the long-wave parameter β defined by $\beta = h_1/\lambda = O(h_2/\lambda)$ is small, the amplitude parameter α defined by $\alpha = a/h_1$ is typically O(1). Therefore, the classical weakly nonlinear assumption of $\alpha \ll 1$ cannot be used.

In order to describe large-amplitude long internal waves, Miyata (1988) and Choi & Camassa (1999) proposed a strongly nonlinear long-wave model, which was derived under the sole assumption of $\beta \ll 1$ while α is assumed to be O(1). The solitary wave solution of the so-called Miyata–Choi–Camassa (MCC) equations valid for the shallow-water case of $h_2/h_1 = O(1)$ has been found to be in good agreement with previous numerical solutions of the Euler equations and experimental observations (Choi & Camassa 1999; Camassa et al. 2006). The MCC equations were also generalized to a two-layer system with a free surface and a multi-layer system (Choi & Camassa 1996; Choi 2000) and their solitary wave solutions have been studied (Barros & Gavrilyuk 2007; Kodaira et al. 2016; Barros, Choi & Milewski 2020; Zhao et al. 2020). A uni-directional model that shares the solitary wave characteristics of the MCC model was also proposed by Choi, Zhi & Barros (2020), although its derivation is heuristic.

While the MCC solitary wave solution predicts well the internal solitary wave characteristics, in particular, for small and large amplitudes, it shows some discrepancy from the Euler solution for intermediate amplitudes although the difference is relatively small (Camassa *et al.* 2006). While the agreement for small amplitudes can be expected, that for large amplitudes is somewhat surprising. For surface waves, as the wave amplitude increases, short-wavelength components are important so that the long-wave assumption becomes invalid. On the other hand, for internal waves, the characteristic wavelength decreases initially with the amplitude to a minimum, but increases to infinity as the wave amplitude approaches its maximum. This implies that the long-wave assumption is valid for small- and large-amplitude waves, but might be less satisfactory for intermediate-amplitude waves. Considering that the MCC equations are the leading-order model truncated at $O(\beta^2)$ under the long-wave assumption of $\beta \ll 1$, one can expect the long-wave expansion to $O(\beta^4)$ or higher to better describe intermediate-amplitude waves.

For surface waves, it has been known that high-order long-wave models can be obtained as a system of two nonlinear evolution equations in infinite series (Agnon, Madsen & Schaffer 1999; Wu 1999, 2001; Madsen, Bingham & Liu 2002; Choi 2019, 2022). One evolution equation is for the surface elevation while the other is for the depth-mean velocity or the velocity at an arbitrary vertical level, including the free surface and the bottom. Depending on the desired accuracy, these models can be truncated at some order of β^2 and studied numerically. However, as shown in Choi (2019), the truncated models can be ill posed at some orders of approximation and such models should be avoided for numerical computations. The only model that is well posed at any order of approximation was shown to be one for the bottom velocity (Choi 2022). It was then shown that the theoretical solutions of the high-order model compare well with Euler solutions and laboratory measurements for large-amplitude solitary waves.

For internal waves, the MCC equations written in terms of the layer-mean velocities have been known to be dynamically unstable due to the wave-induced velocity jump across the interface (Jo & Choi 2002). To avoid this Kelvin–Helmholtz (KH) instability, the time-dependent MCC equations were solved numerically with a filter that removes unstable short-wavelength disturbances, whose wavenumbers are greater than a critical value (Jo & Choi 2008). However, as the internal solitary wave amplitude determines the

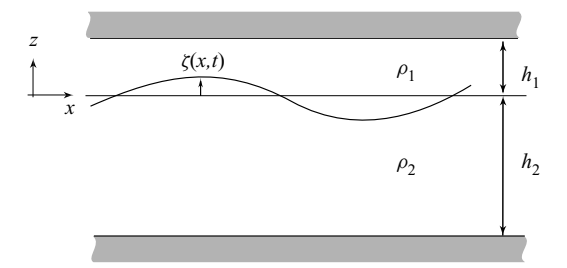


Figure 1. Two-layer system.

critical wavenumber, the filter needs to be adjusted depending on initial conditions and, therefore, is inconvenient to implement for numerical studies.

As an alternative approach, Choi, Barros & Jo (2009) regularized the MCC equations by rewriting the evolution equations in terms of the top and bottom velocities, instead of the layer-mean velocities. The regularized model was also extended to two-dimensional waves by Barros & Choi (2013). Through a local stability analysis, the regularized model was shown to be stable to disturbances of arbitrary wavelengths if the initial solitary wave amplitude is smaller than a critical value, which is close the maximum wave amplitude for a wide range of depth and density ratios (Choi *et al.* 2009). The robustness of the regularized model was then tested numerically using a pseudo-spectral method combined with an iterative scheme (Choi, Goullet & Jo 2011). It is therefore reasonable to choose the top and bottom velocities as dependent variables for a high-order long internal wave model.

Here, using a similar procedure to that introduced in Choi (2022) to obtain the high-order strongly nonlinear long surface wave model, we extend the regularized MCC model written in terms of the top and bottom velocities to an arbitrary order in β^2 and find a high-order solitary wave solution.

The paper is organized as follows. Based on the linear dispersion relations for different long-wave models presented in § 2, a high-order long internal wave model for the shallow-water configuration is obtained for the top and bottom velocities in § 3. Using the second-order model, the leading-order correction to the MCC solitary wave solution is obtained and the resulting solitary wave solutions are compared with the Euler solutions in § 4. After a local stability analysis is presented for the second-order model in § 5, concluding remarks are given in § 6.

2. Basic formulations for long internal waves

At the interface between two fluids of densities ρ_i with i=1 and 2 for the upper and lower layers, respectively, as shown in figure 1, the boundary conditions written in terms of the interface variables are given (Taklo & Choi 2020) by

$$\zeta_t + \nabla \Phi_i \cdot \nabla \zeta = (1 + |\nabla \zeta|^2) W_i, \tag{2.1a}$$

$$\Phi_{it} + \frac{1}{2} |\nabla \Phi_i|^2 + g\zeta = -P/\rho_i + \frac{1}{2} (1 + |\nabla \zeta|^2) W_i^2, \tag{2.1b}$$

where $\zeta(x,t)$ is the interface displacement; $\Phi_i(x,t) = \phi_i(x,z=\zeta,t)$ (i=1,2) are the velocity potentials evaluated at the interface; $W_i(x,t)$ are the vertical velocities evaluated at the interface defined by $W_i = \phi_{i_z|z=\zeta}$; P(x,t) is the pressure at the interface; g is the gravitational acceleration. For static stability, $\rho_2 > \rho_1$ is assumed. Here the subscripts t and t represent partial differentiations with respect to time and the vertical

coordinate, respectively, and ∇ is the two-dimensional horizontal gradient given by $\nabla = (\partial/\partial x, \partial/\partial y)$.

To write (2.1) as a closed system for (ζ, Φ_i, P) , one needs to express W_i in terms of these variables. This closure is similar to that for surface waves in Choi (2022), but is repeated here as some details are worth noting.

2.1. Linear models

For small-amplitude waves, the boundary conditions (2.1) can be linearized to

$$\zeta_t = W_i, \quad \Phi_{it} + g\zeta = -P_i/\rho_i. \tag{2.2a,b}$$

Here, Φ_i and W_i can be approximated by those evaluated at the mean interface (z = 0) so that $\Phi_i(x, t) \simeq \phi_i(x, 0, t) = \phi_{i_0}(x, t)$ and $W_i(x, t) \simeq \partial \phi_i/\partial z|_{z=0} = w_{i_0}(x, t)$.

When the three-dimensional Laplace equations are solved for ϕ_i (i = 1, 2) with the top and bottom boundary conditions given by $\partial \phi_1/\partial z|_{z=h_1} = 0$ and $\partial \phi_2/\partial z|_{z=-h_2} = 0$, respectively, their solutions can be written, in Fourier space, as

$$\hat{\phi}_i(k, z, t) = \{\cosh[k(z + (-1)^i h_i)] / \cosh(kh_i)\} \hat{\phi}_{i_0}(k, t), \tag{2.3}$$

where $\hat{f}(k, z, t)$ is the Fourier transform of f(x, z, t), k = |k| with k being the two-dimensional wavenumber vector and h_1 and h_2 are the thicknesses of the upper and lower layers, respectively. Then, from (2.3), one can obtain

$$\hat{w}_{i_0}(\mathbf{k}, t) = (-1)^i (k \tanh kh_i) \hat{\phi}_{i_0}(\mathbf{k}, t), \tag{2.4}$$

from which the approximate expressions for $W_i \simeq w_{i_0}$ are given, in terms of $\Phi_i \simeq \phi_{i_0}$, by

$$\hat{W}_i(\mathbf{k}, t) \simeq (-1)^i (k \tanh k h_i) \hat{\Phi}_i(\mathbf{k}, t). \tag{2.5}$$

Finally, after taking the Fourier transform of (2.2) and using (2.5), the four linear equations for ζ , Φ_i (i = 1, 2) and P are given, in Fourier space, by

$$\hat{\zeta}_t = (-1)^i (k \tanh kh_i) \hat{\Phi}_i, \quad \hat{\Phi}_{i_t} + g\hat{\zeta} = -\hat{P}/\rho_i. \tag{2.6a,b}$$

Assuming $(\hat{\zeta}, \hat{\Phi}_i, \hat{P}) \sim \exp(-i\omega t)$, the coupled system (2.6) yields the full linear dispersion relation for internal gravity waves (Lamb 1932)

$$\omega^2 = \frac{(\rho_2 - \rho_1)gk \tanh kh_1 \tanh kh_2}{\rho_1 \tanh kh_2 + \rho_2 \tanh kh_1},$$
(2.7)

where the wave frequency ω is always real.

For long waves in shallow water with $kh_i \ll 1$ and $h_1/h_2 = O(1)$, one can expand $T_i = \tanh kh_i$ as

$$T_i = \sum_{n=0}^{\infty} \frac{2^{2n+2}(2^{2n+2}-1)B_{2n+2}}{(2n+2)!} (kh_i)^{2n+1}, \tag{2.8}$$

where B_{2n} are the Bernoulli numbers given by $B_0 = 1$, $B_2 = 1/6$, $B_4 = -1/30$, $B_6 = 1/42$, \cdots .

When the upper limit for the summation in (2.8) is replaced by an integer $M \ge 0$, one can find a truncated linear system given, from (2.6), by

$$\hat{\zeta}_t = (-1)^i k T_{i,M} \hat{\Phi}_i, \quad \hat{\Phi}_{i,t} + g \hat{\zeta} = -\hat{P}/\rho_i,$$
 (2.9*a,b*)

where $T_{i,M}$ represents the Mth-order long-wave approximation of T_i valid to $O(\beta^{2M+1})$ with $kh_i = O(\beta)$. The linear dispersion relation of this truncated system can be found as

$$\omega^2 = \frac{(\rho_2 - \rho_1)gkT_{1,M}T_{2,M}}{\rho_1 T_{2,M} + \rho_2 T_{1,M}}.$$
(2.10)

For example, for M = 2, the dispersion relation is given by

$$\omega^{2} = \frac{(\rho_{2} - \rho_{1})gk^{2}h_{1}h_{2}[1 - \frac{1}{3}(kh_{1})^{2} + \frac{2}{15}(kh_{1})^{4}][1 - \frac{1}{3}(kh_{2})^{2} + \frac{2}{15}(kh_{2})^{4}]}{\rho_{2}h_{1}[1 - \frac{1}{3}(kh_{1})^{2} + \frac{2}{15}(kh_{1})^{4}] + \rho_{1}h_{2}[1 - \frac{1}{3}(kh_{2})^{2} + \frac{2}{15}(kh_{2})^{4}]},$$
 (2.11)

whose right-hand side is positive so that ω is always real. On the other hand, under the leading-order approximation (M=1), or by neglecting terms proportional to $(kh_i)^4$ in (2.11), its right-hand side becomes negative for large k values. If this happens, ω is purely imaginary so that the system is unstable and its imaginary part represents the growth rate. In general, the system for the interface potentials Φ_i is stable for even M while that for odd M is unstable. The same observation was made for surface waves in Choi (2022).

It should be stressed that this discussion about stability of the linear system (2.6) or its long-wave approximation (2.9) is limited to perturbations to the flat interface without background currents. When the interface is no longer flat, different horizontal velocities are induced in the top and bottom layers. Due to this velocity discontinuity across the interface, short-wavelength disturbances are expected to grow by the KH instability mechanism (Jo & Choi 2002). As we are interested in large-amplitude internal waves, the stability of a deformed interface should be examined, but its analysis will be postponed until a high-order long-wave model is obtained.

Instead of the interface potentials, the long-wave model, such as the MCC model, is often written in terms of the layer-mean velocities \bar{u}_i defined by

$$\bar{\mathbf{u}}_1 = \frac{1}{(h_1 - \zeta)} \int_{\zeta}^{h_1} \nabla \phi_1 \, dz, \quad \bar{\mathbf{u}}_2 = \frac{1}{(h_2 + \zeta)} \int_{-h_2}^{\zeta} \nabla \phi_2 \, dz.$$
 (2.12*a,b*)

For small-amplitude waves, after replacing ζ by 0 in the limit of the integration and using (2.3), the Fourier transforms of \bar{u}_i can be approximated by $\hat{\bar{u}}_i \simeq -ik \tanh kh_i/(kh_i)\hat{\Phi}_i$, from which we have $h_i \widehat{\nabla} \cdot \bar{u}_i \simeq -k \tanh kh_i\hat{\Phi}_i$. Then, from (2.9), the linear system for ζ , \bar{u}_i and P can be found, in Fourier space, as

$$\hat{\zeta}_t = (-1)^{i+1} h_i \widehat{\nabla \cdot \bar{u}_i}, \quad kh_i \coth kh_i \hat{\bar{u}}_{i_t} + g \widehat{\nabla \zeta} = -\widehat{\nabla P}/\rho_i. \tag{2.13a,b}$$

Once again, for long waves, when truncated at $O(\beta^{2M})$, the linear system (2.13) yields the following dispersion relation:

$$(\rho_1 h_2 K_{1,M} + \rho_2 h_1 K_{2,M}) \omega^2 = (\rho_2 - \rho_1) g k^2 h_1 h_2, \tag{2.14}$$

where $K_{i,M}$ are the truncated series of $K_i = kh_i \coth kh_i$ given by

$$K_{i,M} = \left[1 + \frac{1}{3}(kh_i)^2 - \frac{1}{45}(kh_i)^4 + \dots + \frac{2^{2M}B_{2M}}{(2M)!}(kh_i)^{2M}\right]. \tag{2.15}$$

Contrary to the system for the surface velocity potentials Φ_i , the system for the layer-mean velocities \bar{u}_i is stable for odd M, but is unstable for even M.

To regularize the MCC model that is ill posed when the interface is deformed, Choi *et al.* (2009) used the velocity potentials at the top and bottom boundaries in the long-wave model. For small-amplitude waves, the interface potentials Φ_i and the velocity potentials evaluated at the rigid top and bottom boundaries $\varphi_i(x, t) = \varphi_i(x, z = (-1)^{i+1}h_i, t)$ are related, from (2.3), as

$$\hat{\Phi}_i \simeq \hat{\phi}_{i_0}(\mathbf{k}, t) = \cosh(kh_i)\hat{\varphi}_i(\mathbf{k}, t). \tag{2.16}$$

Then, from (2.6) with (2.16), the four linear equations for $\hat{\zeta}$, $\hat{\varphi}_i$ (i = 1, 2) and \hat{P} can be obtained as

$$\hat{\zeta}_t = (-1)^i (k \sinh kh_i) \hat{\varphi}_i, \quad (\cosh kh_i) \hat{\varphi}_{i,} + g\hat{\zeta} = -\hat{P}/\rho_i. \tag{2.17a,b}$$

For $kh_i = O(\beta) \ll 1$, when the expansions for $C_i = \cosh kh_i$ and $S_i = \sinh kh_i$ are truncated at $O(\beta^{2M})$, as before, the dispersion relation for (2.17) is given by

$$\omega^2 = \frac{(\rho_2 - \rho_1)gkS_{1,M}S_{2,M}}{\rho_1C_{1,M}S_{2,M} + \rho_2S_{1,M}C_{2,M}},$$
(2.18)

where $C_{i,M}$ and $S_{i,M}$ are the truncated series of C_i and S_i , respectively, given by

$$C_{i,M} = \left[1 + \frac{(kh_i)^2}{2!} + \dots + \frac{(kh_i)^{2M}}{(2M)!}\right],$$
 (2.19a)

$$S_{i,M} = kh_i \left[1 + \frac{(kh_i)^2}{3!} + \dots + \frac{(kh_i)^{2M}}{(2M+1)!} \right].$$
 (2.19b)

As the right-hand side of (2.18) is always positive for any values of k and M, the wave frequency ω is always real. Unlike that for the interface velocity potentials Φ_i or the layer-mean velocities \bar{u}_i , the system for the top and bottom velocity potentials φ_i given by (2.17) is stable, at any order of approximation, to all small disturbances on the flat surface. Therefore, the top and bottom velocity potentials φ_i are chosen to write a high-order long-wave system.

2.2. Nonlinear models

Similarly to Choi (2022), we sketch briefly the derivation of a high-order long-wave model for φ_i . First we expand the three-dimensional velocity potentials $\phi_i(x, z, t)$ (i = 1, 2) in Taylor series about fixed vertical levels, or $z = z_{i\alpha}$

$$\phi_{i}(x, z, t) = \sum_{j=0}^{\infty} \frac{(-1)^{j} (z - z_{i_{\alpha}})^{2j}}{(2j)!} \nabla^{2j} \phi_{i} \bigg|_{z = z_{i_{\alpha}}} + \sum_{j=0}^{\infty} \frac{(-1)^{j} (z - z_{i_{\alpha}})^{2j+1}}{(2j+1)!} \nabla^{2j+1} \cdot \nabla^{-1} \left. \frac{\partial \phi_{i}}{\partial z} \right|_{z = z_{i_{\alpha}}}.$$
 (2.20)

By introducing in (2.20)

$$\phi_{i\alpha} = \phi_i|_{z=z_{i\alpha}}, \quad w_{i\alpha} = \partial \phi_i/\partial z|_{z=z_{i\alpha}},$$
 (2.21*a,b*)

 $\phi_i(x, z, t)$ and $w_i(x, z, t) = \partial \phi_i / \partial z$ can be written (Madsen et al. 2002; Choi 2022) as

$$\phi_i = \cos[(z - z_{i_\alpha})\nabla]\phi_{i_\alpha} + \sin[(z - z_{i_\alpha})\nabla] \cdot \nabla^{-1}w_{i_\alpha}, \qquad (2.22a)$$

$$w_i = -\sin[(z - z_{i_\alpha})\nabla] \cdot \nabla \phi_{i_\alpha} + \cos[(z - z_{i_\alpha})\nabla] w_{i_\alpha}. \tag{2.22b}$$

For finite-amplitude long waves in shallow water, when we choose $z_{i\alpha} = h_1$ and $-h_2$ for i = 1 and 2, respectively, (2.22) can be rewritten, with $w_{i\alpha} = 0$ at the flat top and bottom boundaries, as

$$\phi_i(x, z, t) = \cos[(z + (-1)^i h_i) \nabla] \varphi_i, \quad w_i(x, z, t) = -\sin[(z + (-1)^i h_i) \nabla] \cdot \nabla \varphi_i,$$
(2.23a,b)

where $\varphi_1(x, t)$ and $\varphi_2(x, t)$ are the velocity potentials evaluated at the top and bottom boundaries, respectively. When $z = \zeta$ is substituted into (2.23), Φ_i and W_i can be expressed, in terms of ζ and φ_i , as

$$\Phi_i = \cos[(\zeta + (-1)^i h_i) \nabla] \varphi_i, \quad W_i = -\sin[(\zeta + (-1)^i h_i) \nabla] \cdot \nabla \varphi_i. \tag{2.24a,b}$$

Then, substituting (2.24) into (2.1) yields formally a system of nonlinear evolution equations for ζ and φ_i (i = 1, 2) along with an additional unknown P, although the cosine and sine functions in (2.24) need to be expanded in infinite series and, then, truncated to a certain order in β^2 for practical applications, as discussed in § 3.

Once the high-order long-wave model for φ_i is found, one can obtain a similar model for the interface velocity potentials Φ_i or for the layer-mean velocities \bar{u}_i using the relationships between these variables, as shown in Appendices A and B. However, as mentioned previously, the long-wave model for Φ_i or \bar{u}_i should be used with care as it is stable about the zero states only when truncated at even or odd orders in β^2 , respectively. Furthermore, when the interface is deformed, both models suffer from the KH instability.

3. Regularized high-order model for the top and bottom potentials

3.1. Expansion in terms of the top and bottom velocity potentials

Following Choi (2022), by expanding the cosine and sine functions in (2.24), Φ_i and W_i can be expressed, in terms of ζ and φ_i , as

$$\Phi_i = \sum_{m=0}^{\infty} \Phi_{i,2m}, \quad \Phi_{i,2m} = \frac{(-1)^m}{(2m)!} \eta_i^{2m} \nabla^{2m} \varphi_i, \tag{3.1a,b}$$

$$W_{i} = \sum_{m=0}^{\infty} W_{i,2m}, \quad W_{i,2m} = (-1)^{i} \frac{(-1)^{m+1}}{(2m+1)!} \eta_{i}^{2m+1} \nabla^{2(m+1)} \varphi_{i}, \tag{3.2a,b}$$

where both $\Phi_{i,2m}$ and $W_{i,2m}$ explicitly depend only on ζ and φ_i , and η_i (i=1,2) are defined by

$$\eta_i = h_i + (-1)^i \zeta. \tag{3.3}$$

Assuming that $\eta_i \nabla = O(h_i/\lambda) = O(\beta) \ll 1$ with $\zeta/h_i = O(a/h_i) = O(\alpha) = O(1)$, one can notice that $\Phi_{i,2m}/\Phi_i = O(\beta^{2m})$ and $W_{i,2m}/|\nabla \Phi_i| = O(\beta^{2m+1})$ for $m \ge 0$. Although no small parameter is explicitly introduced, these series can be considered asymptotic series in β^2 when truncated.

3.2. System of nonlinear evolution equations

By substituting (3.1)–(3.2) into (2.1), the nonlinear evolution equations for ζ , P and φ_i can be obtained as

$$\zeta_t = \sum_{m=0}^{\infty} Q_{i,2m}(\zeta, \varphi_i), \quad \Phi_{it} = -P/\rho_i + \sum_{m=0}^{\infty} R_{i,2m}(\zeta, \varphi_i),$$
 (3.4a,b)

where Φ_i are given, in terms of ζ and φ_i , by (3.1). In (3.4), $Q_{i,2m}$ ($m \ge 0$) are given by

$$Q_{i,0} = -\nabla \zeta \cdot \nabla \Phi_{i,0} + W_{i,0}, \tag{3.5a}$$

$$Q_{i,2m} = -\nabla \zeta \cdot \nabla \Phi_{i,2m} + W_{i,2m} + |\nabla \zeta|^2 W_{i,2(m-1)} \quad \text{for } m \ge 1,$$
 (3.5b)

while $R_{i,2m}$ ($m \ge 0$) are given by

$$\mathbf{R}_{i,0} = -g\zeta - \frac{1}{2}|\nabla \Phi_{i,0}|^2, \quad \mathbf{R}_{i,2} = -\nabla \Phi_{i,0} \cdot \nabla \Phi_{i,2} + \frac{1}{2}(W_{i,0})^2, \quad (3.6a,b)$$

$$R_{i,2m} = -\frac{1}{2} \sum_{j=0}^{m} \nabla \Phi_{i,2j} \cdot \nabla \Phi_{i,2(m-j)} + \frac{1}{2} \sum_{j=0}^{m-1} W_{i,2j} W_{i,2(m-j-1)}$$

$$+\frac{1}{2}|\nabla\zeta|^2 \sum_{i=0}^{m-2} W_{i,2j}W_{i,2(m-j-2)} \quad \text{for } m \ge 2.$$
 (3.6c)

In (3.4), both $Q_{i,2m}$ and $R_{i,2m}$ are $O(\beta^{2m})$ for $m \ge 0$.

When the expressions for $\Phi_{i,2m}$ and $W_{i,2m}$ given by (3.1)–(3.2) are substituted into (3.5)–(3.6), one can find the explicit expressions of $Q_{i,2m}$ and $R_{i,2m}$ in terms of ζ and φ_i . In particular, it is useful to notice that $Q_{i,2m}$ can be rewritten as

$$Q_{i,2m} = (-1)^{i} \nabla \cdot \left[\frac{(-1)^{m+1}}{(2m+1)!} \eta_i^{2m+1} \nabla^{2m} \nabla \varphi_i \right] \quad \text{for } m \ge 0.$$
 (3.7)

As (3.4b) is the evolution equation for Φ_i , an additional step is necessary to find φ_i from Φ_i . When the infinite series for Φ_i in (3.1) are inverted, φ_i can be expressed, in terms of ζ and Φ_i , as

$$\varphi_i = \sum_{m=0}^{\infty} \varphi_{i,2m}, \quad \varphi_{i,0} = \Phi_i, \tag{3.8a,b}$$

$$\varphi_{i,2m} = \sum_{i=1}^{m} \frac{(-1)^{j+1}}{(2j)!} \eta_i^{2j} \nabla^{2j} \varphi_{i,2(m-j)} \quad \text{for } m \ge 1.$$
 (3.8c)

3.3. Energy

After eliminating the pressure at the interface P, (3.4) can be rewritten as

$$\zeta_t = \sum_{m=0}^{\infty} Q_{2,2m}(\zeta, \varphi_2), \quad \Psi_t = \sum_{i=1}^{2} (-1)^i \rho_i \sum_{m=0}^{\infty} R_{i,2m}(\zeta, \varphi_i),$$
 (3.9a,b)

along with

$$\sum_{m=0}^{\infty} Q_{1,2m}(\zeta, \varphi_1) = \sum_{m=0}^{\infty} Q_{2,2m}(\zeta, \varphi_2), \tag{3.10}$$

where Ψ is defined by

$$\Psi = \rho_2 \Phi_2 - \rho_1 \Phi_1. \tag{3.11}$$

In Benjamin & Bridges (1997), it has been shown that the system given by (2.1) can be written as Hamilton's equations

$$\zeta_t = \frac{\delta E}{\delta \Psi}, \quad \varphi_t = -\frac{\delta E}{\delta \zeta},$$
(3.12*a*,*b*)

where $\delta E/\delta \zeta$ and $\delta E/\delta \Psi$ represent the functional derivatives of the total energy E with respect to ζ and Ψ , respectively. Then, the system (3.12) conserves the total energy E given by

$$E = \frac{1}{2} \int [(\rho_2 - \rho_1)g\zeta^2 + \Psi \zeta_t] dx.$$
 (3.13)

After substituting (3.4a) with (3.7) for ζ_t into (3.13) and using (3.11) for Ψ with (3.1) for the expressions for Φ_i , the total energy E can be expanded as

$$E = \sum_{m=0}^{\infty} E_{2m}(\zeta, \varphi_1, \varphi_2),$$
 (3.14)

where $E_{2m} = O(\beta^{2m})$ for $m \ge 0$ are given by

$$E_0 = \frac{1}{2} \int \left[(\rho_2 - \rho_1) g \zeta^2 + \rho_1 \eta_1 \nabla \varphi_1 \cdot \nabla \varphi_1 + \rho_2 \eta_2 \nabla \varphi_2 \cdot \nabla \varphi_2 \right] d\mathbf{x}, \tag{3.15a}$$

$$E_{2m} = \frac{1}{2} \sum_{i=1}^{2} \sum_{j=0}^{m} \int \left[(-1)^{i+m} \rho_i \frac{\eta_i^{2j+1} \nabla^{2j} (\nabla \varphi_i) \cdot \nabla (\eta_i^{2(m-j)} \nabla^{2(m-j)} \varphi_i)}{(2j+1)! (2(m-j))!} \right] dx. \quad (3.15b)$$

3.4. Truncated models

The infinite series on the right-hand sides of the system given by (3.4) need to be truncated for numerical computations. The governing equations for ζ , φ_i and P correct to $O(\beta^{2M})$ are then given by

$$\zeta_t = \sum_{m=0}^{M} Q_{i,2m}(\zeta, \varphi_i), \quad \Phi_{it} = -P/\rho_i + \sum_{m=0}^{M} R_{i,2m}(\zeta, \varphi_i),$$
 (3.16*a,b*)

$$\Phi_i = \sum_{m=0}^{M} \Phi_{i,2m}(\zeta, \varphi_i), \tag{3.16c}$$

where $\Phi_{i,2m}$, $Q_{i,2m}$ and $R_{i,2m}$ given by (3.1), (3.5) and (3.6), respectively, are all $O(\beta^{2m})$. This system will be referred to as the *M*th-order system. As mentioned previously, after solving for Φ_i (3.16*b*), φ_i can be obtained from (3.16*c*), which can be inverted asymptotically, as shown in (3.8), or numerically using an iterative scheme introduced in Choi *et al.* (2011). For a low-order approximation (M = 1 or 2), the numerical approach is preferable as the asymptotic inversion is less accurate.

Under the small-amplitude assumption of $\zeta/h_i = O(a/h_i) \ll 1$, the truncated system (3.16) can be linearized to

$$\zeta_t = (-1)^i S_{i,M}[\varphi_i], \quad C_{i,M}[\varphi_{it}] = -P/\rho_i - g\zeta,$$
 (3.17*a,b*)

where the linear operators $C_{i,M}$ and $S_{i,M}$ are defined in (2.19). Notice that $C_{i,M}[\varphi_i]$ and $S_{i,M}[\varphi_i]$ are the linear approximations to Φ_i and W_i . The linear dispersion relation for

(3.17) is then given by (2.18), which shows that the wave frequency is always real for any choice of k and M.

When the zeroth-order (M = 0) approximation is made to (3.16), we have

$$\zeta_t + (-1)^{-i} \nabla \cdot (\eta_i \nabla \varphi_i) = 0, \quad \varphi_{it} + g\zeta + \frac{1}{2} |\nabla \varphi_i|^2 = -P/\rho_i, \tag{3.18a,b}$$

which are the (non-dispersive) shallow-water equations for a two-layer system.

3.4.1. First-order model

When the leading-order dispersive terms of $O(\beta^2)$ are included, (3.16) can be reduced to the first-order (M=1) system given by

$$\zeta_t + (-1)^i \nabla \cdot \left[\left(\eta_i - \frac{\eta_i^3}{3!} \nabla^2 \right) \nabla \varphi_i \right] = 0,$$
 (3.19a)

$$\left[\left(1 - \frac{\eta_i^2}{2!} \nabla^2 \right) \varphi_i \right]_t + g\zeta + \frac{1}{2} \nabla \varphi_i \cdot \nabla \varphi_i = -\frac{P}{\rho_i} + \nabla \cdot \left(\frac{\eta_i^2}{2!} \nabla^2 \varphi_i \nabla \varphi_i \right). \tag{3.19b}$$

After taking the gradient, the first-order system (3.19) can be written, in terms of the bottom velocity $v_i = \nabla \varphi_i$, as

$$\zeta_t + (-1)^i \nabla \cdot \left[\left(\eta_i - \frac{\eta_i^3}{3!} \nabla^2 \right) \mathbf{v}_i \right] = 0, \tag{3.20a}$$

$$\left[\boldsymbol{v}_{i} - \nabla \left(\frac{\eta^{2}}{2!} \nabla \cdot \boldsymbol{v}_{i}\right)\right]_{t} + \nabla \left(g\zeta + \frac{1}{2}\boldsymbol{v}_{i} \cdot \boldsymbol{v}_{i}\right) = -\frac{P}{\rho_{i}} + \nabla \left[\nabla \cdot \left\{\frac{\eta_{i}^{2}}{2!} (\nabla \cdot \boldsymbol{v}_{i}) \boldsymbol{v}_{i}\right\}\right].$$
(3.20b)

This is the regularized long-wave model of Choi *et al.* (2009) that is asymptotically equivalent to the strongly nonlinear long-wave model for the layer-mean velocities, or the MCC equations. Using the relationship between the bottom velocities v_i and the layer-mean velocities \bar{u}_i given, from (B2), by

$$\mathbf{v}_{i} = \bar{\mathbf{u}}_{i} + \frac{\eta_{i}^{2}}{3!} \nabla^{2} \bar{\mathbf{u}}_{i} + O(\beta^{4}), \tag{3.21}$$

one can show that the system given by (3.20) becomes the MCC equations for the layer-mean velocities \bar{u}_i

$$\zeta_t + (-1)^i \nabla \cdot (\eta_i \bar{\boldsymbol{u}}_i) = 0, \tag{3.22a}$$

$$\bar{\boldsymbol{u}}_{it} + \bar{\boldsymbol{u}}_{i} \cdot \nabla \bar{\boldsymbol{u}}_{i} + g \nabla \zeta = -\frac{P}{\rho_{i}} + \frac{1}{\eta_{i}} \nabla \left[\frac{\eta_{i}^{3}}{3} \{ \nabla \cdot \bar{\boldsymbol{u}}_{it} + \bar{\boldsymbol{u}}_{i} \cdot \nabla (\nabla \cdot \bar{\boldsymbol{u}}_{i}) - (\nabla \cdot \bar{\boldsymbol{u}}_{i})^{2} \} \right].$$
(3.22b)

Here, we have used $\nabla(\nabla \cdot \bar{\boldsymbol{u}}_i) = \nabla^2 \bar{\boldsymbol{u}}_i + O(\beta^2)$ from $\nabla \times \bar{\boldsymbol{u}}_i = O(\beta^2)$, which can be seen from (3.21).

3.4.2. Second-order model

The second-order (M = 2) model correct to $O(\beta^4)$ can be written explicitly, from (3.16), as

$$\zeta_t + (-1)^i \nabla \cdot \left[\left\{ \eta_i - \frac{\eta_i^3}{3!} \nabla^2 + \frac{\eta_i^5}{5!} (\nabla^2)^2 \right\} \nabla \varphi_i \right] = 0,$$
 (3.23*a*)

$$\left[\left\{ 1 - \frac{\eta_i^2}{2!} \nabla^2 + \frac{\eta_i^4}{4!} (\nabla^2)^2 \right\} \varphi_i \right]_t + g\zeta + \frac{1}{2} \nabla \varphi_i \cdot \nabla \varphi_i$$

$$= -\frac{P}{\rho_i} + \nabla \cdot \left(\frac{\eta_i^2}{2!} \nabla^2 \varphi_i \nabla \varphi_i \right) - \nabla \cdot \left[\frac{\eta_i^4}{4!} \nabla \varphi_i (\nabla^2)^2 \varphi_i + \frac{\eta_i^4}{16} \nabla (\nabla^2 \varphi_i)^2 \right]. \quad (3.23b)$$

The total energy truncated at $O(\beta^4)$ is given by $E = E_0 + E_2 + E_4$ with E_{2m} (m = 0, 1, 2) defined, from (3.14)–(3.15), by

$$E_0 = \frac{1}{2} \int [(\rho_2 - \rho_1)g\zeta^2 + \rho_1\eta_1\nabla\varphi_1 \cdot \nabla\varphi_1 + \rho_2\eta_2\nabla\varphi_2 \cdot \nabla\varphi_2] dx, \qquad (3.24a)$$

$$E_2 = \frac{1}{3!} \sum_{i=1}^{2} (-1)^i \rho_i \int \eta_i^3 [(\nabla^2 \varphi_i)^2 - \nabla \varphi_i \cdot \nabla^2 \nabla \varphi_i] \, \mathrm{d}x, \tag{3.24b}$$

$$E_4 = \frac{1}{5!} \sum_{i=1}^{2} (-1)^i \rho_i \int \eta_i^5 [3\nabla^2 (\nabla \varphi_i) \cdot \nabla^2 (\nabla \varphi_i) - 4(\nabla^4 \varphi_i)(\nabla^2 \varphi_i) + \nabla \varphi_i \cdot \nabla^4 \nabla \varphi_i] \, dx.$$
(3.24c)

It should be mentioned that, unlike that for the surface velocity potentials or the layer-mean velocities, the truncated system given by (3.23) conserves the truncated total energy only asymptotically.

4. Solitary wave solution

4.1. Wave profile

For one-dimensional travelling waves, after introducing X = x - ct with c being the solitary wave speed, (3.4a) with (3.7) can be integrated into

$$-c\zeta = (-1)^{i} \sum_{m=0}^{\infty} \frac{(-1)^{m+1}}{(2m+1)!} \eta_{i}^{2m+1} D^{2m} [v_{i}] \quad \text{for } m \ge 0,$$

$$(4.1)$$

where D = d/dX and $v_i(X) = D\varphi_i$. As the right-hand side of (4.1) is equivalent to $(-1)^{i+1}\eta_i\bar{u}_i$, it can be seen that we have imposed $(\zeta,\bar{u}_i) \to 0$ as $X \to -\infty$ to obtain (4.1). Note that (4.1) can be inverted to find the expressions for v_i , in terms of ζ , as

$$v_i = \sum_{m=0}^{\infty} v_{i,2m}^s, \quad v_{i,0}^s = (-1)^i \frac{c\zeta}{\eta_i},$$
 (4.2*a*,*b*)

$$v_{i,2m}^s = \sum_{j=1}^m \frac{(-1)^{j+1}}{(2j+1)!} \eta_i^{2j} D^{2j} [v_{i,2(m-j)}^s] \quad m \ge 1.$$
 (4.2c)

Then, from (3.1)–(3.2), the new expressions for Φ_i and W_i can be found, in terms of ζ , as

$$\Phi_{i} = \sum_{m=0}^{\infty} \Phi_{i,2m}^{s}, \quad \Phi_{i,2m}^{s} = \sum_{j=0}^{m} \frac{(-1)^{j}}{(2j)!} \eta_{i}^{2j} D^{2j-1} [v_{i,2(m-j)}^{s}], \tag{4.3a,b}$$

$$W_{i} = \sum_{m=0}^{\infty} W_{i,2m}^{s}, \quad W_{i,2m}^{s} = (-1)^{i} \sum_{j=0}^{m} \frac{(-1)^{j+1}}{(2j+1)!} \eta_{i}^{2j+1} D^{2j+1} [v_{i,2(m-j)}^{s}].$$
 (4.4*a*,*b*)

After substituting these into the steady form of (3.4b) given by

$$-c\rho_i\Phi_{iX} = -P + \rho_i \sum_{m=0}^{\infty} \mathbf{R}_{i,2m}^s(\zeta,\varphi_i), \tag{4.5}$$

and subtracting these two equations (i = 1, 2) from each other to eliminate P, one can find an ordinary differential equation for $\zeta(X)$ as

$$\sum_{i=1}^{2} \sum_{m=0}^{\infty} (-1)^{i} \rho_{i} F_{i,2m}(\zeta; c) = 0, \quad F_{i,2m}(\zeta; c) = cD[\Phi_{i,2m}^{s}] + R_{i,2m}^{s}, \tag{4.6a,b}$$

where $F_{i,2m} = O(\beta^{2m})$ with $R_{i,2m}^s$ given, from (3.6), by

$$R_{i,0}^{s} = -g\zeta - \frac{1}{2}(D[\Phi_{i,0}^{s}])^{2}, \quad R_{i,2}^{s} = -(D[\Phi_{i,0}^{s}])(D[\Phi_{i,2}^{s}]) + \frac{1}{2}(W_{i,0}^{s})^{2}, \qquad (4.7a,b)$$

$$R_{i,2m}^{s} = -\frac{1}{2}\sum_{j=0}^{m}(D[\Phi_{i,2j}^{s}])(D[\Phi_{i,2(m-j)}^{s}]) + \frac{1}{2}\sum_{j=0}^{m-1}W_{i,2j}^{s}W_{i,2(m-j-1)}^{s}$$

$$+\frac{1}{2}(D[\zeta])^{2}\sum_{i=0}^{m-2}W_{i,2j}^{s}W_{i,2(m-j-2)}^{s} \quad \text{for } m \ge 2. \qquad (4.7c)$$

For m = 0, 1, 2, the explicit expressions for $F_{2,2m}$ in (4.6) are given by

$$F_{2,0}(\zeta;c) = \frac{1}{2}\zeta \left(\frac{2c^2}{\eta_2} - \frac{c^2\zeta}{\eta_2^2} - 2g\right),\tag{4.8a}$$

$$F_{2,2}(\zeta;c) = \frac{c^2 h_2^2}{6\eta_2^2} (\zeta'^2 - 2\eta_2 \zeta''), \tag{4.8b}$$

$$F_{2,4}(\zeta;c) = -\frac{c^2 h_2^2}{90\eta_2^2} (12\zeta'^4 - 48\eta_2 \zeta'' \zeta'^2 + 4\eta_2^2 \zeta''' \zeta' + 2\eta_2^3 \zeta'''' + 3\eta_2^2 \zeta''^2).$$
 (4.8c)

The expressions for $F_{1,2m}(\zeta;c)$ (m=0,1,2) can be found from (4.8) by replacing (g,ζ,h_2) by $(-g,-\zeta,h_1)$.

After multiplying by ζ' , (4.6) can be integrated once with respect to X to have the following nonlinear ordinary differential equation

$$\sum_{i=1}^{2} \sum_{m=0}^{\infty} (-1)^{i} \rho_{i} N_{i,2m}(\zeta;c) = 0, \quad N_{i,2m}(\zeta;c,h_{i}) = \int_{-\infty}^{X} F_{i,2m}(\zeta;c) \zeta_{X'} dX'. \quad (4.9a,b)$$

Once again, the explicit expressions for $N_{2,2m}$ (m = 0, 1, 2) are given by

$$N_{2,0}(\zeta;c) = \frac{\zeta^2}{2\eta_2}(c^2 - g\eta_2), \tag{4.10a}$$

$$N_{2,2}(\zeta;c) = -\frac{c^2 h_2^2}{6\eta_2} \zeta'^2, \tag{4.10b}$$

$$N_{2,4}(\zeta;c) = -\frac{c^2 h_2^2}{90\eta_2} (2\eta_2^2 \zeta' \zeta''' - \eta_2^2 \zeta''^2 + 2\eta_2 \zeta'^2 \zeta'' - 12\zeta'^4), \tag{4.10c}$$

where we have imposed $\zeta^{(n)} \to 0$ as $X \to -\infty$ for $n \ge 0$. Note that $N_{1,2m}$ can be found by multiplying $N_{2,2m}$ by -1 and replacing (g, ζ, η_2, h_2) by $(-g, -\zeta, \eta_1, h_1)$.

To find an asymptotic solitary wave solution, we expand c and ζ as

$$c = \sum_{m=0}^{\infty} c_{2m}, \quad \zeta = \sum_{m=0}^{\infty} \zeta_{2m}(X),$$
 (4.11*a,b*)

where both c_{2m} and ζ_{2m} are assumed to be $O(\beta^{2m})$. When these expansions are substituted into (4.9), the zeroth-order approximation, or $\sum_{i=1}^{2} (-1)^{i} \rho_{i} N_{i,0}(\zeta; c) = 0$, yields a trivial solution, or $\zeta = 0$ by imposing the zero boundary conditions at $X = -\infty$. This implies that $-\rho_{1}N_{1,0}(\zeta; c) + \rho_{2}N_{2,0}(\zeta; c) = O(\beta^{2})$ and, therefore, one should include the $O(\beta^{2})$ -terms for a non-trivial solution of (4.9).

4.1.1. First-order solution

The ordinary differential equation that appears at $O(\beta^2)$ is given, from (4.9), by

$$\sum_{i=1}^{2} (-1)^{i} \rho_{i} [N_{i,0}(\zeta_{0}; c_{0}) + N_{i,2}(\zeta_{0}; c_{0})] = 0, \tag{4.12}$$

or

$$\zeta_0^{\prime 2} = \frac{3\zeta_0^2 [(\rho_1 \eta_{2_0} + \rho_2 \eta_{1_0}) c_0^2 - (\rho_2 - \rho_1) g \eta_{1_0} \eta_{2_0}]}{(\rho_1 h_1^2 \eta_{2_0} + \rho_2 h_2^2 \eta_{1_0}) c_0^2} \equiv G(\zeta_0), \tag{4.13}$$

where ζ_0 and c_0 will be referred to as the first-order solutions, and η_{i_0} (i=1,2) are defined by

$$\eta_{i_0} = h_i + (-1)^i \zeta_0. \tag{4.14}$$

Equation (4.13) is the steady version of the MCC equations. From $\zeta'_0 = 0$ at $\zeta_0 = a$, the leading-order wave speed c_0 and the amplitude a are related (Choi & Camassa 1999) as

$$c_0^2 = \frac{(\rho_2 - \rho_1)g(h_1 - a)(h_2 + a)}{\rho_1(h_2 + a) + \rho_2(h_1 - a)},$$
(4.15)

from which the linear long-wave speed c_{lin} can be found, with a=0, as

$$c_{lin}^2 = \frac{(\rho_2 - \rho_1)gh_1h_2}{\rho_1h_2 + \rho_2h_1}. (4.16)$$

For the one-layer case with $\rho_1 = 0$, (4.13) can be reduced to

$${\zeta_0'}^2 = \left(\frac{3g}{c_0^2 h_2^2}\right) \zeta_0^2 \left[\frac{c_0^2}{g} - (h_2 + \zeta_0)\right].$$
 (4.17)

As shown in Choi (2022), this is the first-order equation for solitary waves on the surface of a single layer of thickness h_2 first obtained by Rayleigh (1876) and its solution is given by $\zeta(X) = a \operatorname{sech}^2(k_s X)$ and $c_0^2 = g(h_2 + a)$, where $(k_s h_2)^2 = 3a/[4(h_2 + a)]$ with a being the wave amplitude.

It was shown in Choi & Camassa (1999) that the width of the internal solitary wave solution increases with the wave amplitude and a front solution appears at the maximum amplitude a_m satisfying

$$\rho_1(h_2 + a_m)^2 = \rho_2(h_1 - a_m)^2, \quad \text{or, explicitly,} \quad a_m = \frac{h_1\sqrt{\rho_2/\rho_1} - h_2}{\sqrt{\rho_2/\rho_1} + 1}, \quad (4.18a,b)$$

for which the maximum wave speed is given, from (4.10c), by

$$c_m^2 = g(h_1 + h_2) \left(\frac{\sqrt{\rho_2/\rho_1} - 1}{\sqrt{\rho_2/\rho_1} + 1} \right).$$
 (4.19)

Note that the front solution for $a = a_m$ represents a heteroclinic orbit that connects two fixed points of (4.13) located at $\zeta_0 = 0$ and a_m .

4.1.2. Second-order solution

By substituting (4.11) into (4.9) and collecting terms of $O(\beta^{2m})$, one can find an equation for ζ_{2m} $(m \ge 1)$ as

$$f_1(X)\zeta_{2m}' + f_2(X)\zeta_{2m} = f_3(X)c_{2m} + f_4(X), \tag{4.20}$$

where f_4 is a known function of ζ_{2l} and c_{2l} (l = 0, 1, ..., m - 1) while f_j (j = 1, 2, 3), depending only on the leading-order solutions $(\zeta_0 \text{ and } c_0)$, are given by

$$f_{1} = \sum_{i=1}^{2} (-1)^{i} \rho_{i} \left. \frac{\partial N_{i}}{\partial \zeta'} \right|_{0}, \quad f_{2} = \sum_{i=1}^{2} (-1)^{i} \rho_{i} \left. \frac{\partial N_{i}}{\partial \zeta} \right|_{0}, \quad f_{3} = \sum_{i=1}^{2} (-1)^{i} \rho_{i} \left. \frac{\partial N_{i}}{\partial c} \right|_{0}, \quad (4.21a-c)$$

with $N_i = N_{i,0} + N_{i,2}$ and subscript 0 representing evaluation at $(\zeta, c) = (\zeta_0, c_0)$. Using (4.10a)–(4.10b) for $N_{2,0}$ and $N_{2,2}$ and the similar expressions for $N_{1,0}$ and $N_{1,2}$, one can

find explicitly the following expressions for f_i (i = 1, 2, 3)

$$\zeta_0' f_1 = -\zeta_0^2 [(\rho_1 \eta_{20} + \rho_2 \eta_{10}) c_0^2 - (\rho_2 - \rho_1) g \eta_{10} \eta_{20}], \tag{4.22a}$$

$$f_{2} = -\frac{1}{6}c_{0}^{2}(\rho_{1}h_{1}^{2} - \rho_{2}h_{2}^{2})G(\zeta_{0}) + c_{0}^{2}(\rho_{1}h_{2} + \rho_{2}h_{1})\zeta_{0} - \frac{3}{2}c_{0}^{2}(\rho_{2} - \rho_{1})\zeta_{0}^{2} - (\rho_{2} - \rho_{1})gh_{1}h_{2}\zeta_{0} + \frac{3}{2}(\rho_{2} - \rho_{1})g(h_{2} - h_{1})\zeta_{0}^{2} + 2(\rho_{2} - \rho_{1})g\zeta_{0}^{3},$$

$$(4.22b)$$

$$f_3 = -(\rho_2 - \rho_1)g\eta_{1_0}\eta_{2_0}\zeta_0^2/c_0. \tag{4.22c}$$

The solution of (4.20) is formally given by

$$\zeta_{2m} = \frac{1}{f_0} \int_0^X f_0 \left(\frac{f_3}{f_1} c_2 + \frac{f_4}{f_1} \right) dX' + \frac{C}{f_0}, \quad f_0(X) = \exp \left[\int (f_2/f_1) dX \right], \quad (4.23a,b)$$

where the integrating factor f_0 can be found, from (4.23b) with (4.22), as

$$f_0 = 1/\zeta_0'$$
. (4.24)

As the solitary wave is assumed to be an even function decaying to zero as $X \to \pm \infty$ (except for $a = a_m$, for which the front solution is found), the homogeneous solution of (4.20) given by $C\zeta'_0$ is an odd function decaying at infinities and will be therefore neglected. Note that X = 0 is chosen for the lower limit of the integration in (4.23a). With this choice, ζ_{2m} are always zero at X = 0 and the solitary wave amplitude a remains unchanged with the order of approximation.

At $O(\beta^2)$, the expression for f_4 that depends on ζ_0 and c_0 is given by

$$f_4 = [\rho_1 N_{1_4}(\zeta_0, c_0) - \rho_2 N_{2_4}(\zeta_0, c_0)] \eta_{1_0} \eta_{2_0}, \tag{4.25}$$

where N_{i_4} are given by (4.10c) for i = 2 and the similar expression for i = 1, as explained previously. In evaluating f_4 , the following expressions for the derivatives of ζ_0 would be useful

$${\zeta_0'}^2 = G(\zeta_0), \quad {\zeta_0''} = \frac{1}{2}G'(\zeta_0), \quad {\zeta_0'''} = \frac{1}{2}{\zeta_0'}G''(\zeta_0),$$
 (4.26*a-c*)

where $G'(\zeta_0) = dG/d\zeta_0$ and $G''(\zeta_0) = d^2G/d\zeta_0^2$ with $G(\zeta_0)$ defined by (4.13). Unlike the surface wave case in Choi (2022), this expression for f_4 is so complex that (4.23*a*) needs to be evaluated numerically.

After rewriting (4.23) with C = 0 and $d\zeta_0 = \zeta_0' dX$ as

$$\zeta_{2m} = \frac{1}{f_0} \int_a^{\zeta_0} f_0 \left(\frac{f_3}{f_1} c_2 + \frac{f_4}{f_1} \right) \frac{\mathrm{d}\zeta_0}{\zeta_0'},\tag{4.27}$$

we first determine c_2 by removing the (non-integrable) singularity of the integrand at the lower limit, or $\zeta_0 = a$. From the following asymptotic behaviour of the integrand near

 $\zeta_0 = a$

$$\left(\frac{f_0 f_3}{\zeta_0' f_1}, \frac{f_0 f_4}{\zeta_0' f_1}\right) = \frac{(\mu_1, \nu_1)}{|\zeta_0 - a|^{3/2}} + \frac{(\mu_2, \nu_2)}{|\zeta_0 - a|^{1/2}} + O(|\zeta_0 - a|^{1/2}),$$
(4.28)

with μ_j and ν_j (j=1,2) being constants, the leading-order singularity at $\zeta_0 = a$ can be removed by choosing c_2 to be $c_2 = -\nu_1/\mu_1$, which can be found explicitly as

$$\frac{c_2}{c_0} = -\frac{a^2(\rho_1 h_1^2 \eta_{1_a} + \rho_2 h_2^2 \eta_{2_a})(\rho_1 \eta_{2_a}^2 - \rho_2 \eta_{1_a}^2)^2}{40 \eta_{1_a} \eta_{2_a}(\rho_1 \eta_{2_a} + \rho_2 \eta_{1_a})(\rho_1 h_1^2 \eta_{2_a} + \rho_2 h_2^2 \eta_{1_a})^2},$$
(4.29)

where $\eta_{i_a} = h_i + (-1)^i a$ (i = 1, 2). As $\rho_1 \to 0$, this can be reduced to the result for surface waves on a single layer with the thickness h_2 (Choi 2022)

$$\frac{c_2}{c_0} = -\frac{a(h_2 + a)}{40h_2^2}\gamma,\tag{4.30}$$

where $c_0 = [g(h_2 + a)]^{1/2}$ and $\gamma = a/(h_2 + a)$ is the smallness parameter used in the expansion.

Notice that c_2 in (4.29) vanishes at the maximum wave amplitude $a = a_m$, for which $\rho_1 \eta_{2a}^2 - \rho_2 \eta_{1a}^2 = 0$. This implies that the maximum wave speed predicted by the first-order (MCC) equations is indeed the exact solution of the Euler equations, as shown in Choi & Camassa (1999). Although no correction to the wave speed c_0 at $a = a_m$ is necessary so that $c_{2m} = 0$, the corresponding MCC solution for the wave profile is different from the exact solution of the Euler equations, in particular, in the transition region between the two constant states ($\zeta = 0$ and $\zeta = a_m$).

Figure 2 shows the variation of the wave speed c with the amplitude |a| for the density and depth ratios given by $\rho_2/\rho_1 = 1.022$ and $h_2/h_1 = 4.132$, respectively. These physical parameters were used to compute the solitary wave profiles in Camassa et~al.~(2006) to validate the MCC solution with the numerical solution of the Euler equations for the shallow configuration. The improvement for the wave speed by the second-order solution is relatively small as the first-order MCC solution c_0 given by (4.10c) predicts well the wave speed for the entire range of wave amplitudes, $0 \le |a| \le |a_m|$, where the maximum amplitude a_m/h_1 is approximately -1.552. Nevertheless, one can see that the first-order solution slightly overpredicts the wave speed, and the second-order solution $c = c_0 + c_2 + O(\beta^4)$ with c_2 given explicitly by (4.29) clearly improves the comparison with the Euler solution.

To find ζ_2 , (4.27) with c_2 given by (4.29) needs to be computed numerically. To accurately evaluate the integral, we rewrite (4.27) as

$$\zeta_2 = \frac{1}{f_0} \left[2(\mu_2 c_2 + \nu_2) \sqrt{|\Delta a|} + \int_{a - \Delta a}^{\zeta_0} F(z) \, \mathrm{d}z \right],\tag{4.31a}$$

$$F(\zeta_0) = \frac{f_0}{\zeta_0'} \left(\frac{f_3}{f_1} c_2 + \frac{f_4}{f_1} \right), \tag{4.31b}$$

where the first term is $O(|\Delta a|^{1/2})$ and represents the (approximate) evaluation of the integral from z=a to $z=a-\Delta a$ with $|\Delta a/a|\ll 1$, where Δa is a small shift away from a (integrable) singularity at z=a. The integration in (4.31a) is evaluated numerically with $|\Delta a|/h_1=10^{-10}$ using an integration routine 'NIntegrate' in the Mathematica (Wolfram Research, Inc., v.12). The computed ζ_2 as a function of ζ_0 is shown in figure 3 for four different wave amplitudes. Similarly to the wave speed, the second-order correction is still

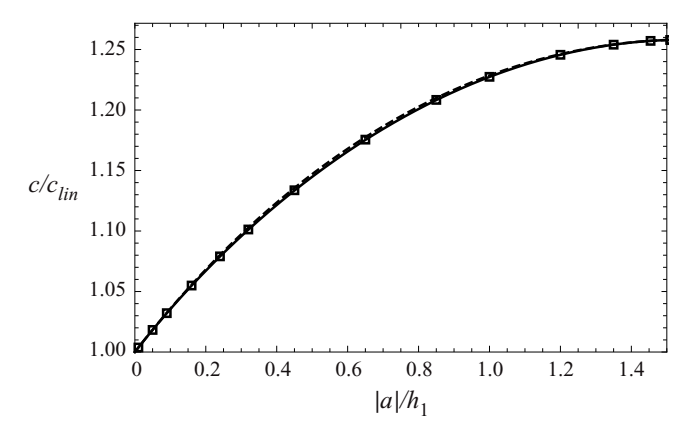


Figure 2. Solitary wave speed c vs amplitude |a|. The second-order (solid line) solution $c = c_0 + c_2 + O(\beta^4)$ is compared with the Euler solution (Camassa et al. 2006) (open squares) and the first-order solution (dashed line) $c = c_0 + O(\beta^2)$, where c_0 and c_2 are given by (4.10c) and (4.29), respectively. Here, c_{lin} is the linear wave speed given by (4.11a,b), the density and depth ratios are given by $\rho_2/\rho_1 = 1.022$ and $h_2/h_1 = 4.132$, respectively, and the maximum amplitude is $|a_m|/h_1 \simeq 1.552$.

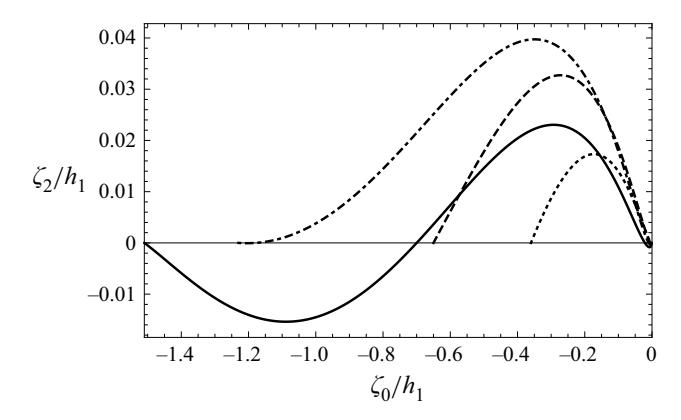


Figure 3. Numerical evaluation of (4.27) for ζ_2 parameterized by ζ_0 for four different solitary wave amplitudes of depression: $|a|/h_1 = 0.36$ (dotted), 0.65 (dashed); 1.23 (dot-dashed); 1.51 (solid). Here, the density and depth ratios are given by $\rho_2/\rho_1 = 1.022$ and $h_2/h_1 = 4.132$, respectively.

small. For $|a|/h_1 = 0.36$, 0.65 and 1.23, as ζ_2 is positive while ζ_0 is negative for solitary waves of depression, the second-order solution would lie above the first-order solution except for $\zeta_0 = 0$ and $\zeta_0 = a$, where $\zeta_2 = 0$. On the other hand, for $|a|/h_1 = 1.51$ close to the maximum wave amplitude, ζ_2 is positive for smaller values of $|\zeta_0|$, but is negative near the maximal displacement at $\zeta_0 = a$.

The computed second-order wave profiles given by $\zeta = \zeta_0 + \zeta_2 + O(\beta^4)$ for $|a|/h_1 = 0.36, 0.65, 1.23, 1.51$ are shown in figure 4 and are indistinguishable from the Euler solutions. As shown in Choi & Camassa (1999) and Camassa *et al.* (2006), the first-order MCC solutions are close to the Euler solutions over a wide range of wave amplitudes, but the improvement made by ζ_2 can be clearly seen for intermediate wave amplitudes.

Figure 5 shows the effective wavelength λ defined by

$$\lambda = \left| \frac{1}{a} \int_0^\infty \zeta(X) \, dX \right| = \lambda_0 + \lambda_2 + O(\beta^4), \tag{4.32}$$

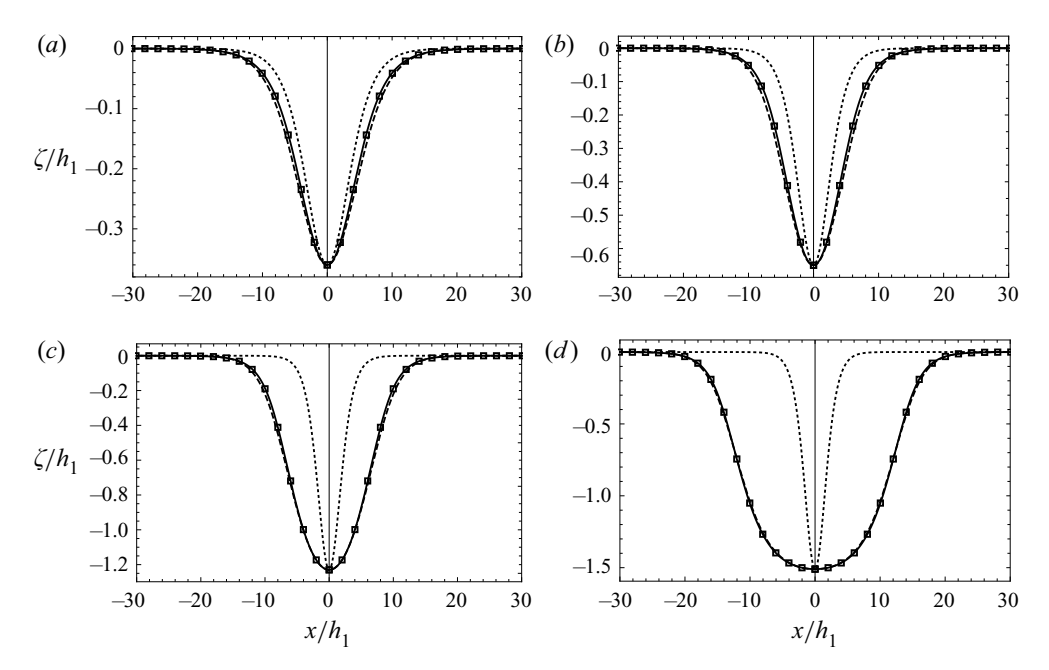


Figure 4. Comparison of internal solitary wave profiles for four different wave amplitudes: (a) $a/h_1 = -0.36$; (b) -0.65; (c) -1.23; (d) -1.51. The second-order solitary wave solution (solid) given by $\zeta = \zeta_0 + \zeta_2 + O(\beta^4)$ is compared with the Euler solution (Camassa *et al.* 2006) (open squares), the first-order (MCC) solution ζ_0 (dashed) and the weakly nonlinear (Koretweg–de Vries, KdV) solution (dotted). Here, the density and depth ratios are given by $\rho_2/\rho_1 = 1.022$ and $h_2/h_1 = 4.132$, respectively.

where λ_{2m} (m = 0, 1) are given by

$$\lambda_{2m} = \left| \frac{1}{a} \int_{a}^{0} \zeta_{2m} (d\zeta_0 / \zeta_0') \right|. \tag{4.33}$$

While λ_0 can be explicitly expressed in terms of complete elliptic functions, as shown in Choi & Camassa (1999), λ_2 needs to be computed numerically. Using (4.27) and (4.33) for m=1, the expression for λ_2 can be obtained as

$$\lambda_2 = \left| \frac{1}{a} \int_a^0 \int_a^{\zeta_0} F(z) \, dz \, d\zeta_0 \right|, \tag{4.34}$$

where F(z) is given by (4.31b) with $f_0 = 1/\zeta'_0$. Once again, the 'NIntegrate' routine in the Mathematica has been used to evaluate the integration in (4.34).

As observed in the comparison for the wave profiles, the second-order solution is expected to better predict the effective wavelength λ , particularly for intermediate wave amplitudes. As shown in figure 5, the second-order solution indeed agrees well with the Euler solution for the entire range of wave amplitudes, $0 \le |a| \le |a_m|$. Therefore, for long internal waves in the shallow-water configuration, the second-order long-wave solution is expected to be sufficient and no higher-order approximation seems to be necessary for practical applications.

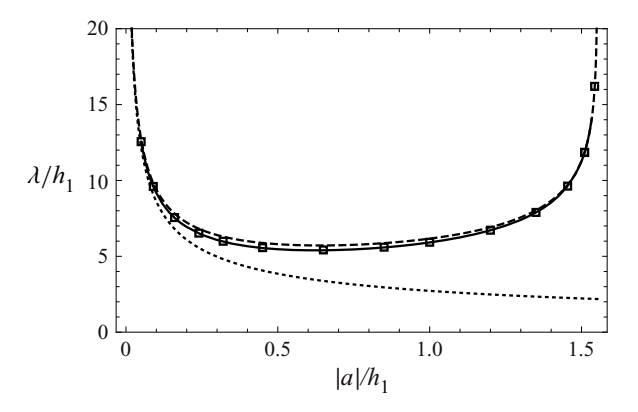


Figure 5. Effective wavelength λ vs wave amplitude |a|. The second-order solution (solid) is compared with the Euler solution (Camassa *et al.* 2006) (open squares), the first-order (MCC) solution (dashed) and the weakly nonlinear (KdV) solution (dotted). Here, the density and depth ratios are given by $\rho_2/\rho_1 = 1.022$ and $h_2/h_1 = 4.132$, respectively.

4.2. Velocity field induced by a solitary wave

The horizontal and vertical velocities, $(u_i, w_i) = (\phi_{iX}, \phi_{iz})$, induced by a solitary wave can be computed, from (2.23), as

$$u_i(X, z) = \sum_{m=0}^{\infty} \frac{(-1)^m}{(2m)!} [z + (-1)^i h_i]^{2m} D^{2m} v_i,$$
 (4.35a)

$$w_i(X, z) = \sum_{m=0}^{\infty} \frac{(-1)^{m+1}}{(2m+1)!} [z + (-1)^i h_i]^{2m+1} D^{2m+1} v_i, \tag{4.35b}$$

where $\zeta \le z \le h_1$ for i=1 and $-h_2 \le z \le \zeta$ for i=2. To find the asymptotically consistent velocity field, the top and bottom velocities $v_i(X) = \varphi_{iX}$ should be first expanded as

$$v_i = \sum_{m=0}^{\infty} v_{i,2m}^s,$$
 (4.36)

where $v_{i,2m}^s = O(\beta^{2m})$ can be found by substituting into (4.2) the expansions for ζ and c given by (4.11). After substituting (4.36) into (4.35), one can find the following expressions of u_i and w_i

$$u_i(X,z) = \sum_{m=0}^{\infty} u_{i,2m}^s(X,z), \quad u_{i_{2m}}^s = \sum_{j=0}^m \frac{(-1)^j}{(2j)!} [z + (-1)^i h_i]^{2j} D^{2j} v_{i,2(m-j)}^s, \quad (4.37a,b)$$

$$w_i(X, z) = \sum_{m=0}^{\infty} w_{i,2m}^s(X, z), \tag{4.38a}$$

$$w_{i,2m}^{s} = \sum_{j=0}^{m} \frac{(-1)^{j+1}}{(2j+1)!} [z + (-1)^{i} h_{i}]^{2j+1} D^{2j+1} v_{i,2(m-j)}^{s}, \tag{4.38b}$$

where $u_{i,2m}^s$ and $w_{i,2m}^s$ are both $O(\beta^{2m})$.

With the following expressions for $v_{i,2m}^{s}$ (m = 0, 1)

$$v_{i,0}^s = (-1)^i \frac{c_0 \zeta_0}{\eta_{i_0}},\tag{4.39a}$$

$$v_{i,2}^{s} = c_0 \left[(-1)^{i} \left(\frac{c_2}{c_0} \frac{\zeta_0}{\eta_{i_0}} + \frac{h_i \zeta_2}{\eta_{i_0}^2} \right) + \frac{\eta_{i_0}^2}{6} \left(\frac{h_i \eta_{i_0}^{"}}{\eta_{i_0}^2} - \frac{2h_i \eta_{i_0}^{"}}{\eta_{i_0}^3} \right) \right], \tag{4.39b}$$

the horizontal velocity of the *i*th layer u_i correct to $O(\beta^2)$ is given explicitly by

$$u_{i}(X,z) = c_{0} \left[(-1)^{i} \left(\frac{\zeta_{0}}{\eta_{i_{0}}} + \frac{c_{2}}{c_{0}} \frac{\zeta_{0}}{\eta_{i_{0}}} + \frac{h_{i}\zeta_{2}}{\eta_{i_{0}}^{2}} \right) + \left(\frac{\eta_{i_{0}}^{2}}{6} - \frac{(z + (-1)^{i}h_{i})^{2}}{2} \right) \left(\frac{h_{i}\eta_{i_{0}}^{"}}{\eta_{i_{0}}^{2}} - \frac{2h_{i}\eta_{i_{0}}^{"}}{\eta_{i_{0}}^{3}} \right) \right],$$
(4.40)

where the expressions for c_{2m} and ζ_{2m} (m = 0, 1) have been found in § 4.1.

Figure 6 shows the horizontal velocities u_i at X = 0 (at the location of the maximal displacement) given by

$$u_i(0,z) = (-1)^i c_0 \left[\frac{\zeta_0}{\eta_{i_0}} + \frac{c_2}{c_0} \frac{\zeta_0}{\eta_{i_0}} + \left(\frac{\eta_{i_0}^2}{6} - \frac{(z + (-1)^i h_i)^2}{2} \right) \left(\frac{h_i \zeta_0''}{\eta_{i_0}^2} \right) \right]_{X=0}^{l}, \quad (4.41)$$

where $\zeta_2 = \zeta_0' = 0$ at X = 0 have been used and ζ_0'' can be computed, from (4.26b), as $\zeta_0'' = G'[\zeta_0]/2$. Here, to better represent the variation in the vertical z direction, note that $|u_i|$ are shown. Again, the second-order solution agrees well with the Euler solution for all wave amplitudes. As discussed previously, the correction c_2 to the leading-order wave speed c_0 is so small that the second term proportional to c_2 in (4.39b) is negligible. Therefore, the expressions for $u_i(0, z)$ without the second term used in Camassa et al. (2006) are good approximations to the second-order solution although they are asymptotically inconsistent.

The maximum horizontal velocity jump across the interface occurs at the location of the maximal displacement, or X = 0, and can be found, from (4.39b) with z = a, as

$$U_2 - U_1 = (c_0 + c_2) \frac{a(h_1 + h_2)}{(h_1 - a)(h_2 + a)} - \frac{c_0}{6} G'(a)(h_1 + h_2), \tag{4.42}$$

where $U_i = u_i(0, a)$. As shown in figure 7, the velocity jump for the second-order solitary wave solution is slightly greater than that for the first-order solution. Due to this increased velocity jump, the second-order internal solitary wave could be more unstable by the KH instability mechanism (Jo & Choi 2002) and its stability needs to be examined when it is perturbed by short-wavelength disturbances.

5. Local stability analysis for the high-order system

When a solitary wave is perturbed by short-wavelength disturbances, one can perform a local stability analysis by assuming that the variations of the internal solitary wave and the wave-induced currents are slow and can be neglected over the characteristic wavelength of

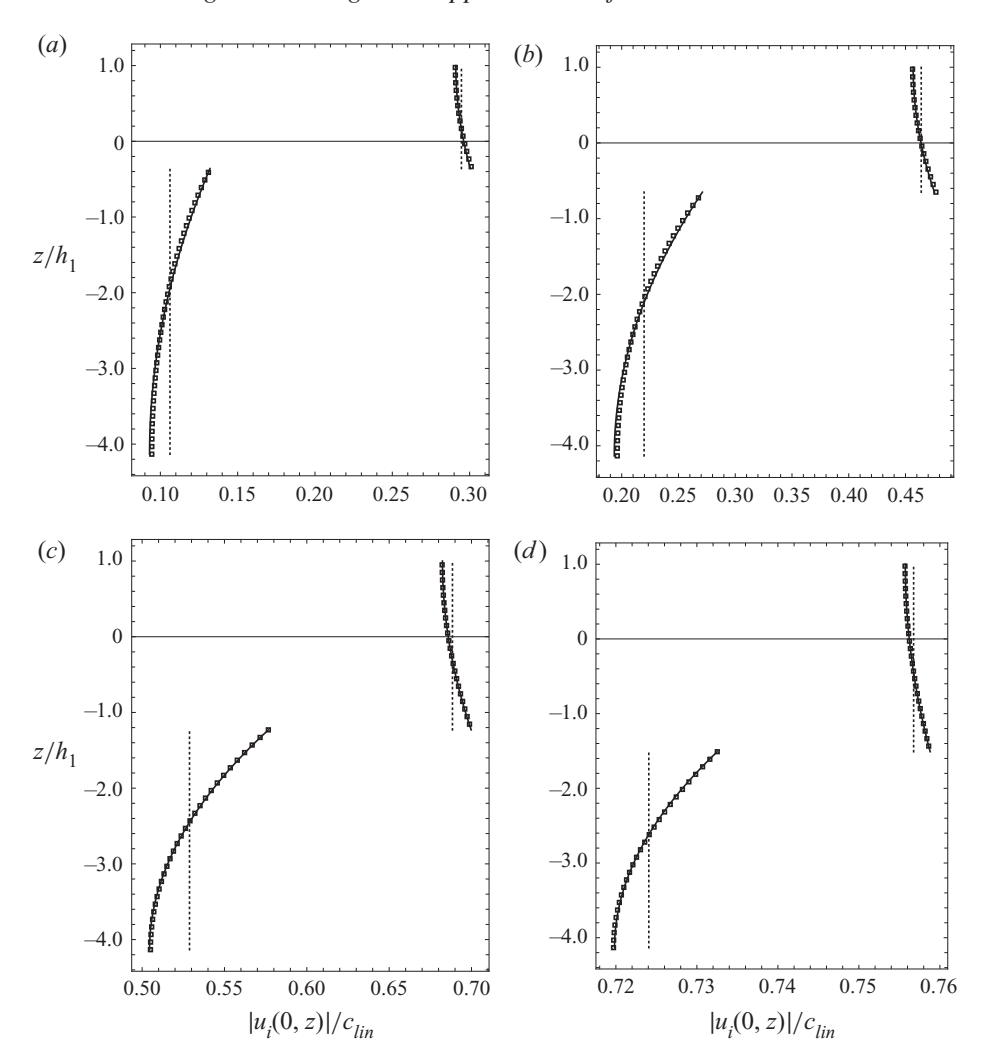


Figure 6. Comparison of $|u_i(0, z)|$ for four different wave amplitudes: (a) $a/h_1 = -0.36$; (b) -0.65; (c) -1.23; (d) -1.51. The second-order solitary wave solution (solid) given by (4.39a) is compared with the Euler solution (Camassa *et al.* 2006) (open squares) and the mean velocity $|u_i| = |v_{i_0}^s|$ (dotted). Notice that $u_1 = |u_1|$ and $u_2 = -|u_2|$ for solitary waves propagating to the right. Here, the density and depth ratios are given by $\rho_2/\rho_1 = 1.022$ and $h_2/h_1 = 4.132$, respectively.

the disturbances. For the local stability analysis, ζ and φ_i are perturbed about a and $U_i x$ so that they can be written as

$$\zeta = a + \zeta', \quad \varphi_i = U_i x + \varphi_i', \quad P = P_0 + P',$$
 (5.1*a-c*)

where U_i and P_0 represent the current in the *i*th layer and the interface pressure induced by the solitary wave, respectively. In (5.1), all perturbations are assumed small so that $|\zeta'/a| \ll 1$, $|\varphi'_{ix}/U_i| \ll 1$, and $|P'/P_0| \ll 1$. Then, with the following expressions for ζ' and φ'_i

$$(\zeta', \varphi_i', P') = (\hat{\zeta}, \hat{\varphi}_i, \hat{P}) e^{i(kx - \omega t)}, \tag{5.2}$$

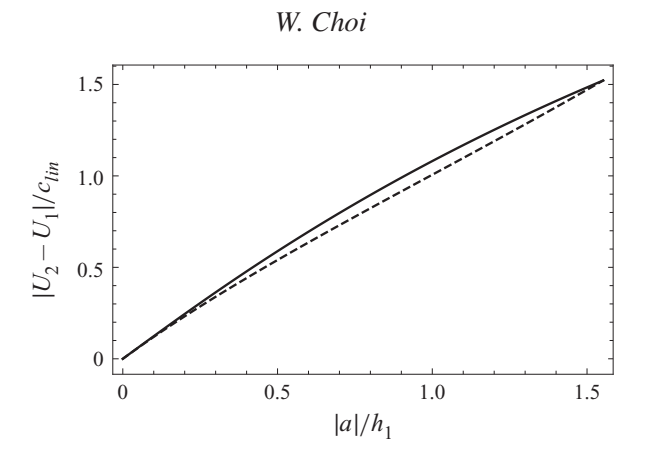


Figure 7. The velocity jump across the interface $|U_2 - U_1|$ vs the wave amplitude |a|: The second-order solution (solid) is compared with the first-order (MCC) solution (dashed) for the density and depth ratios given by $\rho_2/\rho_1 = 1.022$ and $h_2/h_1 = 4.132$, respectively.

the second-order system (3.23) can be linearized, after eliminating \hat{P} , to

$$-i(\omega - kU_i)\hat{\zeta} - (-1)^i k^2 H_i A_i \hat{\varphi}_i = 0, \qquad (5.3a)$$

$$\sum_{i=1}^{2} (-1)^{i} \rho_{i} [-i(\omega - kU_{i})B_{i}\hat{\varphi}_{i} + g\hat{\zeta}] = 0,$$
(5.3b)

where A_i and B_i are given by

$$A_i = 1 + \frac{(kH_i)^2}{3!} + \frac{(kH_i)^4}{5!}, \quad B_i = 1 + \frac{(kH_i)^2}{2!} + \frac{(kH_i)^4}{4!},$$
 (5.4a,b)

with H_i defined by

$$H_i = h_i + (-1)^i a. (5.5)$$

From (5.3), the dispersion relation for ω can be obtained as

$$\rho_1 H_2 A_2 B_1 (\omega - kU_1)^2 + \rho_2 H_1 A_1 B_2 (\omega - kU_2)^2 - (\rho_2 - \rho_1) g k^2 H_1 H_2 A_1 A_2 = 0, \quad (5.6)$$

or

$$(\rho_1 H_2 A_2 B_1 + \rho_2 H_1 A_1 B_2) \omega^2 - 2k(\rho_1 H_2 U_1 A_2 B_1 + \rho_2 H_1 U_2 A_1 B_2) \omega$$

+ $k^2 (\rho_1 H_2 U_1^2 A_2 B_1 + \rho_2 H_1 U_2^2 A_1 B_2) - (\rho_2 - \rho_1) g k^2 H_1 H_2 A_1 A_2 = 0.$ (5.7)

For stability, ω has to be real for all possible ranges of physical parameters ρ_i and h_i , which is true only when the discriminant of (5.7), or Δ , is non-negative:

$$\Delta = -\rho_1 \rho_2 H_1 H_2 A_1 A_2 B_1 B_2 (U_2 - U_1)^2 + (\rho_2 - \rho_1) H_1 H_2 A_1 A_2 (\rho_1 H_2 A_2 B_1 + \rho_2 H_1 A_1 B_2) \ge 0,$$
 (5.8)

or

$$|U_2 - U_1|^2 \le g(\rho_2 - \rho_1)g\left(\frac{H_1}{\rho_1}\frac{A_1}{B_1} + \frac{H_2}{\rho_2}\frac{A_2}{B_2}\right).$$
 (5.9)

This condition can be reduced to that for the first-order regularized model obtained by Choi et al. (2009) when the terms proportional to $(kH_i)^4$ are neglected from the expressions for

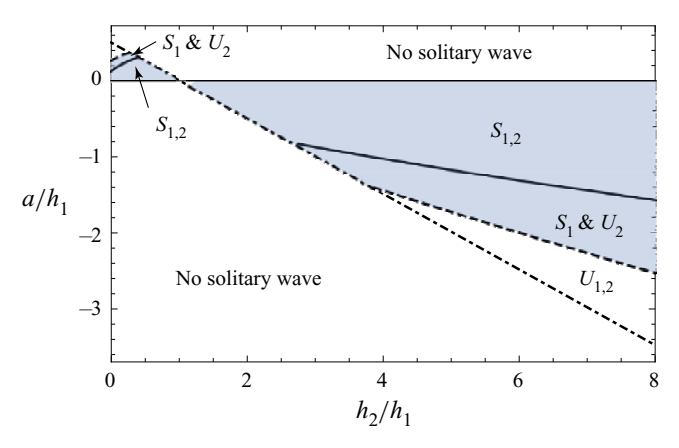


Figure 8. Stability diagram in the (a, h)-plane for $\rho = 1.022$ from the local stability analysis for the firstand second-order models given by (3.19) and (3.23), respectively. The solid and dashed lines represent the critical wave amplitudes for the first- and second-order models, respectively. The dot-dashed line represents the maximum wave amplitude a_m , above (or below) which the solitary wave solution exists when $h > \sqrt{\rho}$ (or $h < \sqrt{\rho}$). The mth-order solitary wave solution is expected to be stable (or unstable) to local short-wavelength disturbances in S_m (or U_m) for the specified range of the wave amplitude a when its propagation is studied numerically with the mth-order model (m = 1, 2).

 A_i and B_i given by (5.4*a,b*). As observed in Choi *et al.* (2009), since A_i/B_i decrease with kH_i monotonically from 1, the maximum velocity jump across the interface allowed for stability for any values of kH_i is determined by the minimum of the right-hand side of (5.9), which happens when $kH_i \to \infty$. Therefore, for given physical parameters (ρ_i , H_i), the stability criterion for the second-order model can be written, from (5.9), as

$$|U_2 - U_1|^2 \le \frac{g(\rho_2 - \rho_1)}{5} \left(\frac{H_1}{\rho_1} + \frac{H_2}{\rho_2}\right).$$
 (5.10)

By substituting into (5.10) the expression for $U_2 - U_1$ in terms of a given by (4.42), one can find the critical wave amplitude a_{cr} . Then, for $|a| \le |a_{cr}|$, the solitary wave is stable, as shown in figure 8. The critical wave amplitude $|a_{cr}|$ for the second-order model is smaller than that for the first-order regularized model of Choi *et al.* (2009), for which the minima of A_i/B_i are 1/3, instead of 1/5. Therefore, the stability criterion for the second-order model is more stringent.

As the solitary wave solution exists up to the maximum amplitude a_m given by (4.18), it is stable for all possible wave amplitudes if the physical parameters satisfy the following inequality

$$(5 - \sqrt{\rho})h^3 - \sqrt{\rho}(12 - 5\sqrt{\rho} + \rho)h^2 - \sqrt{\rho}(1 - 5\sqrt{\rho} + 12\rho)h + \rho^{3/2}(5\sqrt{\rho} - 1) \le 0,$$
(5.11)

where $\rho = \rho_2/\rho_1$ and $h = h_2/h_1$. To obtain (5.11), the expression for $U_2 - U_1$ given by (4.42) has been substituted into (5.10) with $a = a_m$.

Figure 9 shows the region of stability for the second-order model (the shaded region bounded by the solid lines), where ρ and h satisfy the inequality given by (5.11). For any values of ρ and h inside the stable region, the solitary wave is expected to be stable for all possible wave amplitudes, or $0 \le |a| \le |a_m|$. It should be mentioned that, even for the values of ρ and h outside the stability region, the solitary wave is still stable for $|a| \le |a_{cr}|$.

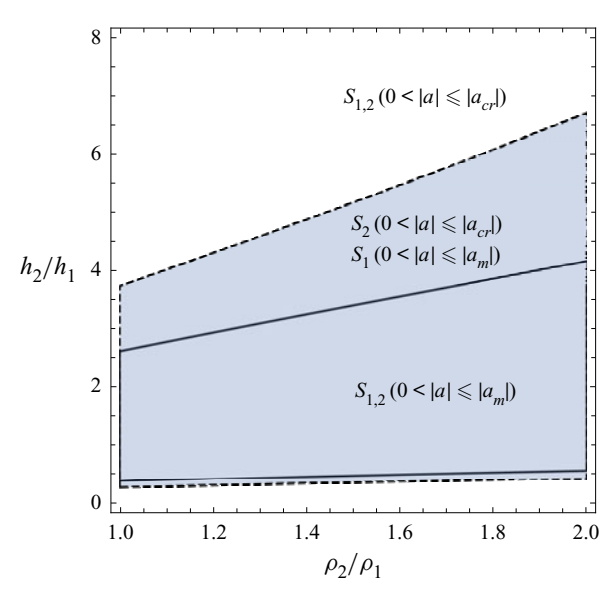


Figure 9. Stability diagram in the (ρ, h) -plane. The first- and second-order solitary waves are stable for all possible amplitudes $(0 \le |a| \le |a_m|)$ inside the shaded regions bounded by the solid and dashed lines, respectively. Notice the stability region for the second-order model is smaller than that for the first-order model of Choi *et al.* (2009).

Compared with the first-order stable region defined (Choi et al. 2009) by

$$(3 - \sqrt{\rho})h^2 - 8\sqrt{\rho}h + 3\rho - \sqrt{\rho} \le 0, (5.12)$$

the second-order model is less stable, as discussed earlier.

In fact, as the dispersion relation for the Mth-order model can be found from (5.6) with

$$A_i = 1 + \frac{(kH_i)^2}{3!} + \dots + \frac{(kH_i)^{2M}}{(2M+1)!}, \quad B_i = 1 + \frac{(kH_i)^2}{2!} + \dots + \frac{(kH_i)^{2M}}{(2M)!}, \quad (5.13a,b)$$

the stability criterion for the Mth-order model is expected to be

$$|U_2 - U_1|^2 \le \frac{g(\rho_2 - \rho_1)}{2M + 1} \left(\frac{H_1}{\rho_1} + \frac{H_2}{\rho_2}\right).$$
 (5.14)

Considering that $|U_2 - U_1|$ increases with the wave amplitude a, as shown in figure 7, the critical wave amplitude $|a_{cr}|$ decreases as M increases and, therefore, the higher-order system is more prone to short-wave instability. However, as the second-order solitary wave solution is sufficiently accurate when compared with the Euler solution, a higher-order model than the second order might be unnecessary.

6. Conclusion

The high-order long-wave approximation adopted for surface waves (Choi 2022) has been applied to internal waves in a system of two layers of different density to obtain a high-order long internal wave model written in terms of the horizontal velocities at the top and bottom boundaries. This is a high-order extension of the regularized model of Choi *et al.* (2009) originally developed to improve the stability characteristics of the MCC equations in the shallow-water configuration.

Using the second-order model, the leading-order correction to the solitary wave solution of the MCC equations has been found. The resulting second-order solutions have been compared with the Euler solutions for the wave profile, the effective wavelength and the vertical profile of the horizontal velocity. While the first-order MCC solutions agree well with the numerical solutions of the Euler equations and laboratory measurements for a wide range of wave amplitudes, some discrepancy was previously observed, in particular, for intermediate wave amplitudes. Considering that the effective wavelength has a minimum at an intermediate amplitude and becomes unbounded as $a \to 0$ or a_m , it is not so surprising that the long-wave approximation is more relevant for waves of small or large amplitudes than those of intermediate amplitudes. It has been found that the leading-order correction removes this discrepancy and the second-order solution compares well with the Euler solution.

It has been known that the inviscid two-layer models including the MCC equations suffer from the KH-type instability caused by the tangential velocity jump across the interface (Jo & Choi 2002, 2008). The local stability analysis for the second-order model has shown that the solitary wave solution is still stable when the wave amplitude is less than a critical value. Although the critical wave amplitude for the second-order model has been found to be smaller than that for the first-order model, it could be still equal or close to the maximum wave amplitude.

In Choi *et al.* (2011), a numerical method based on a pseudo-spectral method along with an iterative scheme to invert a semi-linear operator has been found efficient and stable for the regularized model of Choi *et al.* (2009). This was consistent with the local analysis for the first-order model. As the same numerical method has been applied successfully to the high-order long surface wave model (Choi 2022) that has a mathematical structure similar to that of the internal wave model, it can be also used to solve the time-dependent second-order model for long internal waves, as predicted by its local stability analysis.

It should be pointed out that the high-order long-wave model studied here has been obtained under the assumption of $h_2/h_1 = O(1)$, or for the shallow-water case and, therefore, cannot be applied to the deep-water case of $h_2/h_1 \gg 1$. For the deep-water configuration, the second-order correction to the strongly nonlinear model of Choi & Camassa (1999) has been previously obtained and studied in de Zárate *et al.* (2009), Debsarma, Das & Kirby (2010) and Zhao *et al.* (2016).

Funding. This research was supported by the US National Science Foundation through Grant No. DMS-2108524 and the Brain Pool Program funded by the Ministry of Science and ICT through the National Research Foundation of Korea (Grant No. 2021H1D3A2A01082312).

Declaration of interests. The author reports no conflict of interest.

Author ORCIDs.

Wooyoung Choi https://orcid.org/0000-0002-4433-3013.

Appendix A. Long-wave model for the interface velocity potentials

By inverting (3.1a), φ_i (i = 1, 2) can be expressed, in terms of ζ and Φ_i , as

$$\varphi_i = \sum_{m=0}^{\infty} \tilde{\Phi}_{i,2m}, \quad \tilde{\Phi}_{i,0} = \Phi_i, \tag{A1a,b}$$

$$\tilde{\Phi}_{i,2m} = -\sum_{j=1}^{m} \frac{(-1)^{j}}{(2j)!} \eta_i^{2j} \nabla^{2j} [\tilde{\Phi}_{i,2(m-j)}] \quad \text{for } m \ge 1,$$
(A1c)

where η_i are given (3.3). By substituting (A1) into (3.2), W_i can be found as

$$W_i = \sum_{m=0}^{\infty} \tilde{W}_{i,2m},\tag{A2a}$$

$$\tilde{W}_{i,2m} = (-1)^i \sum_{i=0}^m \frac{(-1)^{j+1}}{(2j+1)!} \eta_i^{2j+1} \nabla^{2(j+1)} [\tilde{\Phi}_{i,2(m-j)}] \quad \text{for } m \ge 0.$$
 (A2b)

By substituting (A2) into (2.1), the nonlinear evolution equations for ζ and Φ_i can be found as

$$\zeta_t = \sum_{m=0}^{\infty} \tilde{Q}_{i,2m}(\zeta, \Phi_i), \quad \Phi_{it} = -P/\rho_i + \sum_{m=0}^{\infty} \tilde{R}_{i,2m}(\zeta, \Phi_i), \quad (A3a,b)$$

where $\tilde{Q}_{i,2m}$ and $\tilde{R}_{i,2m}$ are given by

$$\tilde{\mathbf{Q}}_{i,0} = \tilde{W}_{i,0} - \nabla \tilde{\Phi}_{i,0} \cdot \nabla \zeta, \quad \tilde{\mathbf{Q}}_{i,2m} = \tilde{W}_{i,2m} + |\nabla \zeta|^2 \tilde{W}_{i,2(m-1)} \quad \text{for } m \ge 1, \quad (A4a,b)$$

$$\tilde{\mathbf{R}}_{i,0} = -g\zeta - \frac{1}{2}|\nabla \tilde{\Phi}_{i,0}|^2, \quad \tilde{\mathbf{R}}_{i,2} = \frac{1}{2}\tilde{W}_{i,0}^2, \quad (A.5a,b)$$

$$\tilde{\mathbf{R}}_{i,2m} = \frac{1}{2} \sum_{j=0}^{m-1} \tilde{W}_{i,2j} \tilde{W}_{i,2(m-j-1)} + \frac{1}{2} |\nabla \zeta|^2 \sum_{j=0}^{m-2} \tilde{W}_{i,2j} \tilde{W}_{i,2(m-j-2)} \quad \text{for } m \ge 2.$$
 (A5c)

When the system given by (A3) is truncated at $O(\beta^4)$, one can find the following second-order system for ζ , Φ_i (i = 1, 2) and P

$$(-1)^{i}\zeta_{t} + \nabla \cdot (\eta_{i}\nabla\Phi_{i}) + \nabla^{2}(\frac{1}{3}\eta_{i}^{3}\nabla^{2}\Phi_{i}) + \nabla^{2}[\nabla \cdot (\frac{2}{15}\eta_{i}^{5}\nabla^{2}\nabla\Phi_{i}) + \frac{1}{3}\eta_{i}^{3}\nabla \cdot (\eta_{i}\nabla\eta_{i})(\nabla^{2}\Phi_{i})] = 0,$$

$$(A6a)$$

$$\Phi_{it} + g\zeta + \frac{1}{2}\nabla\Phi_{i} \cdot \nabla\Phi_{i} - \frac{1}{2}\eta_{i}^{2}(\nabla^{2}\Phi_{i})^{2} + \eta_{i}^{2}(\nabla^{2}\Phi_{i})[\nabla^{2}(\frac{1}{2}\eta_{i}^{2}\nabla^{2}\Phi_{i}) + \frac{1}{2}|\nabla\eta_{i}|^{2}\nabla^{2}\Phi_{i} - \frac{1}{6}\eta_{i}^{2}\nabla^{4}\Phi_{i}] = -P/\rho_{i}.$$

$$(A6b)$$

When linearized, this second-order system (A6) yields the linear dispersion relation given by (2.11), which shows that ω is always real and is stable. It should be remembered that the first-order system for the interface variables is unstable. However, as $\omega \sim k^3$ for large k, the time step needs to be small for numerical computations. Therefore, the system might not be so useful when the interface is perturbed by a large-amplitude internal solitary wave.

Appendix B. Long-wave model for the layer-mean velocities

By substituting (2.23*a*) into (2.12), the layer-mean velocities \bar{u}_i can be written, in terms of ζ and φ_i , as

$$\bar{u}_i = \frac{1}{\eta_i} \sin(\eta_i \nabla) \varphi_i = \sum_{m=0}^{\infty} \frac{(-1)^m}{(2m+1)!} \eta_i^{2m} \nabla^{2m} v_i,$$
 (B1)

where $v_i = \nabla \varphi_i$ are the velocities at the top (i = 1) and bottom (i = 2) boundaries. By inverting (B1), the expressions for v_i can be found, in terms of ζ and \bar{u}_i , as

$$\mathbf{v}_i = \sum_{m=0}^{\infty} \bar{\mathbf{v}}_{i,2m}, \quad \bar{\mathbf{v}}_{i,0} = \bar{\mathbf{u}}_i, \tag{B2}a,b)$$

$$\bar{\mathbf{v}}_{i,2m} = \sum_{j=1}^{m} \frac{(-1)^{j+1}}{(2j+1)!} \eta_i^{2j} \nabla^{2j} \bar{\mathbf{v}}_{i,2(m-j)} \quad \text{for } m \ge 1.$$
 (B2c)

From (3.7) and (B1), one can see that the evolution equation for ζ given by (3.4*a*) can be written, at any order of approximation, as

$$\zeta_t + (-1)^i \nabla \cdot (\eta_i \bar{\boldsymbol{u}}_i) = 0, \tag{B3}$$

which represents the exact conservation law of mass.

From (3.1), $V_i = \nabla \Phi_i$ can be expressed, in terms of ζ and $v_i = \nabla \varphi_i$, as

$$V_i = \sum_{m=0}^{\infty} V_{i,2m}(\zeta, \mathbf{v}_i), \quad V_{i,2m} = \nabla \left[\frac{(-1)^m}{(2m)!} \eta_i^{2m} \nabla^{2(m-1)} \nabla \cdot \mathbf{v}_i \right].$$
 (B4a,b)

By substituting (B2) into (B4), V_i can be expressed, in terms of ζ and the layer-mean velocity \bar{u}_i , as

$$V_i = \sum_{m=0}^{\infty} \bar{V}_{i,2m}(\zeta, \bar{\boldsymbol{u}}_i), \tag{B5}$$

where $\bar{V}_{i,0} = \bar{u}_i$ and $\bar{V}_{i,2m}$ $(m \ge 1)$ are given by

$$\bar{V}_{i,2m} = \sum_{j=0}^{m} \frac{(-1)^{j}}{(2j)!} \eta_i^{2j} \nabla^{2j} \bar{\mathbf{v}}_{i,2(m-j)} + \nabla \eta_i \sum_{j=0}^{m-1} \frac{(-1)^{j+1}}{(2j+1)!} \eta_i^{2j+1} \nabla^{2j} \nabla \cdot \bar{\mathbf{v}}_{i,2(m-j-1)}, \quad (B6)$$

with $\bar{v}_{i,2j}$ expressed, in terms of ζ and \bar{u}_i , in (B2).

Then, from (B3) and (3.4b), the evolution equations for ζ and \bar{u}_i can be written as

$$\zeta_t + (-1)^i \nabla \cdot (\eta_i \bar{u}_i) = 0, \quad V_{it} = -\frac{P}{\rho_i} + \sum_{m=0}^{\infty} \nabla \bar{R}_{i,2m}(\zeta, \bar{u}_i),$$
 (B7)

where V_i are given, in terms of ζ and \bar{u}_i , by (B5) with (B6). In (B7), $\bar{R}_{i,2m}$ ($m \ge 0$) are given by

$$\begin{split} \bar{\mathbf{R}}_{i,0} &= -g\zeta - \frac{1}{2}\bar{V}_{i,0} \cdot \bar{V}_{i,0}, \quad \bar{\mathbf{R}}_{i,2} = -\bar{V}_{i,0} \cdot \bar{V}_{i,0} + \frac{1}{2}\bar{W}_{i,0}^{2}, \\ \bar{\mathbf{R}}_{i,2m} &= -\frac{1}{2}\sum_{j=0}^{m} \bar{V}_{i,2j} \cdot \bar{V}_{i,2(m-j)} + \frac{1}{2}\sum_{j=0}^{m-1} \bar{W}_{i,2j}\bar{W}_{i,2(m-j-1)} \\ &+ \frac{1}{2}|\nabla\zeta|^{2}\sum_{j=0}^{m-2} \bar{W}_{i,2j}\bar{W}_{i,2(m-j-2)} \quad \text{for } m \geq 2, \end{split} \tag{B8c}$$

where $\bar{W}_{i,2m}$ are expressed in terms of ζ and \bar{u}_i as

$$\bar{W}_{i,2m} = \sum_{j=0}^{m} \frac{(-1)^{j+1}}{(2j+1)!} \eta_i^{2j+1} \nabla^{2j} \nabla \cdot \bar{\boldsymbol{v}}_{i,2(m-j)}, \tag{B9}$$

with $\bar{v}_{i,2j}$ given by (B2).

When truncated at $O(\beta^2)$, the system given by (B7) becomes the MCC equations given by (3.22) while the next-order approximation will yield the second-order system, or the high-order MCC equations with $\bar{V}_{i,2m}$ and $\bar{R}_{i,2m}$ given by

$$\bar{V}_{i,0} = \bar{\boldsymbol{u}}_i, \quad \bar{V}_{i,2} = -\frac{\eta_i^2}{3} \nabla^2 \bar{\boldsymbol{u}}_i - \eta_i \nabla \eta_i \nabla \cdot \bar{\boldsymbol{u}}_i, \tag{B10a,b}$$

$$\bar{V}_{i,4} = \frac{\eta_i^4}{30} \nabla^4 \bar{\mathbf{u}}_i - \frac{\eta_i^2}{18} \nabla^2 (\eta_i^2 \nabla^2 \bar{\mathbf{u}}_i) - \frac{\eta_i^2}{3} |\nabla \eta_i|^2 \nabla^2 \bar{\mathbf{u}}_i,$$
 (B10c)

$$\bar{R}_{i,0} = -g\zeta - \frac{1}{2}\bar{\boldsymbol{u}} \cdot \bar{\boldsymbol{u}}_i, \tag{B11a}$$

$$\bar{R}_{i,2} = \frac{\eta_i^2}{2} (\nabla \cdot \bar{\boldsymbol{u}}_i)^2 + \bar{\boldsymbol{u}}_i \cdot \left(\frac{\eta_i^2}{3} \nabla^2 \bar{\boldsymbol{u}}_i + \eta_i \nabla \eta_i \nabla \cdot \bar{\boldsymbol{u}}_i \right), \tag{B11b}$$

$$\begin{split} \bar{R}_{i,4} &= -\bar{\boldsymbol{u}}_i \cdot \left[\frac{\eta_i^4}{30} \nabla^4 \bar{\boldsymbol{u}}_i - \frac{\eta_i^2}{18} \nabla^2 (\eta_i^2 \nabla^2 \bar{\boldsymbol{u}}_i) - \frac{\eta_i^2}{3} |\nabla \eta_i|^2 \nabla^2 \bar{\boldsymbol{u}}_i \right] \\ &- \frac{1}{2} \left(\frac{\eta_i^2}{3} \nabla^2 \bar{\boldsymbol{u}}_i + \eta_i \nabla \eta_i \nabla \cdot \bar{\boldsymbol{u}}_i \right)^2 + \frac{\eta_i^3}{3} (\nabla \cdot \bar{\boldsymbol{u}}_i) (\nabla \eta_i \cdot \nabla^2 \bar{\boldsymbol{u}}_i) \\ &+ \frac{1}{2} |\nabla \eta_i|^2 (\eta_i \nabla \cdot \bar{\boldsymbol{u}}_i)^2. \end{split} \tag{B11c}$$

Unfortunately, this second-order system for the layer-mean velocities is linearly unstable when the zero states are perturbed and, therefore, should be avoided for practical applications.

REFERENCES

AGNON, Y., MADSEN, P.A. & SCHAFFER, H.A. 1999 A new approach to high-order Boussinesq models. J. Fluid Mech. 399, 319–333.

BARROS, R. & CHOI, W. 2013 On regularizing the strongly nonlinear model for two-dimensional internal waves. *Physica D* **264**, 27–34.

BARROS, R., CHOI, W. & MILEWSKI, P.A. 2020 Strongly nonlinear effects on internal solitary waves in three-layer flows. *J. Fluid Mech.* 883, A16.

BARROS, R. & GAVRILYUK, S.L. 2007 Dispersive nonlinear waves in two-layer flows with free surface. II. Large amplitude solitary waves embedded into the continuous spectrum. *Stud. Appl. Maths* **119**, 213–251.

BENJAMIN, T.B. & BRIDGES, T.J. 1997 Reappraisal of the Kelvin–Helmholtz problem. Part 1. Hamiltonian structure. *J. Fluid Mech.* 333, 301–325.

CAMASSA, R., CHOI, W., MICHALLET, H., RUSAS, P.O. & SVEEN, J.K. 2006 On the realm of validity of strongly nonlinear asymptotic approximations for internal waves. *J. Fluid Mech.* **549**, 1–23.

CHOI, W. 2000 Modeling of strongly nonlinear internal waves in a multilayer system. In *Proceedings of the Fourth International Conference on Hydrodynamics* (ed. Y. Goda, M. Ikehata & K. Suzuki), pp. 453–458. ICHD2000.

CHOI, W. 2019 On Rayleigh expansion for nonlinear long water waves. J. Hydrodyn. 31, 1115–1126.

CHOI, W. 2022 High-order strongly nonlinear long wave approximation and solitary wave solution. J. Fluid Mech. 945, A15.

- CHOI, W., BARROS, R. & Jo, T.-C. 2009 A regularized model for strongly nonlinear internal solitary waves. J. Fluid Mech. 629, 73–85.
- CHOI, W. & CAMASSA, R. 1996 Weakly nonlinear internal waves in a two-fluid system. J. Fluid Mech. 313, 83–103.
- CHOI, W. & CAMASSA, R. 1999 Fully nonlinear internal waves in a two-fluid system. *J. Fluid Mech.* **396**, 1–36
- CHOI, W., GOULLET, A. & JO, T.-C. 2011 An iterative method to solve a regularized model for strongly nonlinear long internal waves. J. Comp. Phys. 230, 2021–2030.
- CHOI, W., ZHI, C. & BARROS, R. 2020 High-order unidirectional model with adjusted coefficients for large-amplitude long internal waves. *Ocean Model.* 151, 101643.
- DEBSARMA, S., DAS, K.P. & KIRBY, J.T. 2010 Fully nonlinear higher-order model equations for long internal waves in a two-fluid system. *J. Fluid Mech.* **654**, 281–303.
- HELFRICH, K.R. & MELVILLE, W.K. 2006 Long nonlinear internal waves. *Annu. Rev. Fluid Mech.* 38, 395–425.
- JO, T.-C. & CHOI, W. 2002 Dynamics of strongly nonlinear solitary waves in shallow water. Stud. Appl. Math. 109, 205–228.
- JO, T.-C. & CHOI, W. 2008 On stabilizing the strongly nonlinear internal wave model. Stud. Appl. Math. 120, 65–85.
- KODAIRA, T., WASEDA, T., MIYATA, M. & CHOI, W. 2016 Internal solitary waves in a two-fluid system with a free surface. *J. Fluid Mech.* **804**, 201–223.
- LAMB, H. 1932 Hydrodynamics, 6th edn. Dover Publications.
- MADSEN, P.A., BINGHAM, H.B. & LIU, H. 2002 A new approach to high-order Boussinesq models. *J. Fluid Mech.* 462, 1–30.
- MIYATA, M. 1988 Long internal waves of large amplitude. In Proceedings of the IUTAM Symposium on Nonlinear Water Waves (ed. H. Horikawa & H. Maruo), pp. 399–406. Springer Verlag.
- RAYLEIGH, L. 1876 On waves. Phil. Mag. Ser. (5) 1, 257–279.
- TAKLO, T.M.A. & CHOI, W. 2020 Group resonant interactions between surface and internal gravity waves in a two-layer system. J. Fluid Mech. 892, A14.
- Wu, T.Y. 1999 Modeling nonlinear dispersive water waves. J. Eng. Mech. 11, 747–755.
- Wu, T.Y. 2001 A unified theory for modeling water waves. Adv. Appl. Mech. 37, 1–88.
- DE ZÁRATE, A.R., VIGO, D., NACHBIN, A. & CHOI, W. 2009 A higher-order internal wave model accounting for large bathymetric variations. *Stud. Appl. Math.* **122**, 275–294.
- ZHAO, B.B., ERTEKIN, R.C., DUAN, W.Y. & WEBSTER, W.C. 2016 New internal-wave model in a two-layer fluid. J. Waterway, Port, Coastal, Ocean Engng 142, 04015022.
- ZHAO, B.B., WANG, Z., DUAN, W.Y., ERTEKIN, R.C., HAYATDAVOODI, M. & ZHANG, T. 2020 Experimental and numerical studies on internal solitary waves with a free surface. J. Fluid Mech. 899, A17.